

# THE CROSS-CORRELATION OF MGII ABSORPTION AND GALAXIES IN BOSS

IGNASI PÉREZ-RÀFOLS<sup>\*1,2</sup>, JORDI MIRALDA-ESCUDE<sup>1,3</sup>, BRITT LUNDGREN<sup>4,5</sup>, JIAN GE<sup>6</sup>,  
 PATRICK PETITJEAN<sup>7</sup>, DONALD P. SCHNEIDER<sup>8,9</sup>, DONALD G. YORK<sup>10</sup>,  
 AND BENJAMIN A. WEAVER<sup>11</sup>

**ABSTRACT.** We present a measurement of the cross-correlation of MgII absorption and massive galaxies, using the DR11 galaxy sample of the Baryon Oscillation Spectroscopic Survey of SDSS-III, and the DR7 quasar spectra of SDSS-II. The cross-correlation is measured by stacking quasar absorption spectra shifted to the redshift of galaxies that are within a certain impact parameter bin of the quasar, after dividing by a quasar continuum model. This results in an average MgII equivalent width as a function of impact parameter from a galaxy, ranging from 50 kpc to more than 10 Mpc in proper units, which includes all MgII absorbers. We show that special care needs to be taken to use an unbiased quasar continuum estimator, to avoid systematic errors in the measurement of the mean stacked MgII equivalent width. The measured cross-correlation follows the expected shape of the galaxy correlation function, although measurement errors are large. We use the cross-correlation amplitude to derive the bias factor of MgII absorbers, finding  $b_{\text{MgII}} = 1.50 \pm 0.19$ , where the error accounts only for the statistical uncertainty in measuring the mean equivalent width. This result indicates that MgII absorbers at redshift  $z \simeq 0.5$  are spatially distributed on large scales similarly to galaxies with  $L \simeq L_*$ .

**KEYWORDS:** galaxies: haloes, galaxies: formation, quasars: absorption lines, large-scale structure of universe

---

<sup>1</sup>INSTITUT DE CIÈNCIES DEL COSMOS, UNIVERSITAT DE BARCELONA/IEEC, BARCELONA E-08028, CATALONIA.

<sup>2</sup>DEPARTAMENT D'ASTRONOMIA I METEOROLOGIA, FACULTAT DE FÍSICA, UNIVERSITAT DE BACELONA, E-08028 BARCELONA, CATALONIA.

<sup>3</sup>INSTITUCIÓ CATALANA DE RECERCA I ESTUDIS AVANÇATS, BARCELONA, CATALONIA.

<sup>4</sup>DEPARTMENT OF ASTRONOMY, UNIVERSITY OF WISCONSIN - MADISON, 475 NORTH CHARTER STREET, MADISON, WI 53706 USA.

<sup>5</sup>NATIONAL SCIENCE FOUNDATION ASTRONOMY AND ASTROPHYSICS POSTDOCTORAL FELLOW.

<sup>6</sup>DEPARTMENT OF ASTRONOMY, UNIVERSITY OF FLORIDA, BRYANT SPACE SCIENCE CENTER, GAINESVILLE, FL 32611-2055, USA.

<sup>7</sup>INSTITUT D'ASTROPHYSIQUE DE PARIS, UPMC & CNRS, UMR7095 98BIS BOULEVARD ARAGO, 75014 - PARIS, FRANCE.

<sup>8</sup> DEPARTMENT OF ASTRONOMY AND ASTROPHYSICS, THE PENNSYLVANIA STATE UNIVERSITY, UNIVERSITY PARK, PA 16802.

<sup>9</sup> INSTITUTE FOR GRAVITATION AND THE COSMOS, THE PENNSYLVANIA STATE UNIVERSITY, UNIVERSITY PARK, PA 16802.

<sup>10</sup>DEPARTMENT OF ASTRONOMY AND ASTROPHYSICS AND THE ENRICO FERMI INSTITUTE, UNIVERSITY OF CHICAGO, 5640 SOUTH ELLIS AVENUE, CHICAGO, IL 60637, USA.

<sup>11</sup> CENTER FOR COSMOLOGY AND PARTICLE PHYSICS, NEW YORK UNIVERSITY, NEW YORK, NY 10003 USA.

*E-mail addresses:* \*iprafols@icc.ub.edu.

## 1. INTRODUCTION

The MgII doublet absorption line, at rest-frame wavelengths  $\lambda = 2796.3543 \text{ \AA}$  and  $2803.5315 \text{ \AA}$ , is an extremely useful tracer of photoionized gas clouds in galactic halos. Several reasons account for this trait: magnesium is among the most abundant of the heavy elements, the oscillator strength of this MgII doublet is particularly large, its rest-frame wavelength makes it easily observable from ground-based telescopes at redshifts  $z > 0.3$ , and magnesium is mostly in the form of MgII in photoionized, self-shielded clouds at the typical pressures of galactic halos. Gas clouds with atomic hydrogen column densities  $N_{HI} \lesssim 2 \times 10^{17} \text{ cm}^{-2}$  are optically thin to photons above the hydrogen ionization potential of 13.6 eV, as well as to the harder photons that ionize MgII. Most of the magnesium is therefore ionized more than once in thin clouds, greatly reducing the MgII column density. On the other hand, in optically thick clouds, the shielded magnesium ions are mostly recombined to MgI, but MgI has an ionization potential of 7.65 eV (below that of hydrogen) and is ionized by photons that penetrate the region of self-shielded hydrogen. Hence, self-shielded clouds in galactic halos should have most of their magnesium as MgII (e.g., Bergeron & Stasińska, 1986). In fact, most strong MgII systems are also Lyman limit systems, i.e., their HI column densities are high enough to be self-shielding (Rao et al., 2006).

The rest-frame equivalent width distribution of MgII absorption systems is approximated by an exponential form,  $dN/dz \propto \exp(-W/W^*)$ , with a value  $W^* \simeq 0.6 \text{ \AA}$  at  $z = 0.5$  that increases gradually with redshift, and an excess of systems over this form at  $W < 0.3 \text{ \AA}$  (Nestor et al., 2005; Narayanan et al., 2007, and references therein). Most of the strong systems have a complex velocity structure, with a velocity dispersion of multiple absorbing components that is characteristic of galaxy velocity dispersions, favoring models of a collection of photoionized clouds randomly moving through a galactic halo (Bahcall, 1975; Sargent et al., 1979; Churchill et al., 2000), as had already been proposed by Bahcall & Spitzer (1969).

The association of MgII absorption systems with galactic halos was firmly established with the work of Lanzetta & Bowen (1990), Bergeron & Boissé (1991), and Steidel et al. (1994). The observations of the frequency of occurrence of MgII absorbers at different impact parameters from luminous galaxies led to a simple model of halos that are close to spherical, in which absorption with rest-frame equivalent width  $W > 0.3 \text{ \AA}$  is nearly always observed within an impact parameter  $r_p \lesssim 50(L_K/L_K^*)^{0.15} \text{ kpc}$  of a galaxy of K-band luminosity  $L_K$ , and becomes rapidly weaker at larger radii, independently of the type of galaxy being considered (Steidel, 1995). The natural expectation is of a smooth profile of declining mean MgII absorption strength with impact parameter around a galaxy, caused by a decreasing density of clouds with radius in a galactic halo. This result is consistent with more recent work, where the mean MgII equivalent width (which is indicative of the number of intersected individual clumps with saturated absorption) has been shown to steeply decline with the impact parameter  $r_p$  roughly as  $\overline{W} \propto r_p^{-1.5}$  (Chen et al., 2010a), with a characteristic radius at a fixed  $\overline{W}$  that scales proportionally to  $R_{\text{MgII}} \propto M_*^{0.3} (\text{sSFR})^{0.1}$

(Chen et al., 2010b), where  $M_*$  is the stellar mass in the galaxy and sSFR is the star formation rate per unit of stellar mass.

The large extent of the gaseous halos traced by metal absorbers and their ubiquitous presence around all massive galaxies, with only a weak dependence on the specific star formation rate, are observational facts providing support to a scenario in which the MgII absorbers are a signature of the accretion process of new material onto galaxies. Accreting gas at the temperatures of virialization in galactic halos is thermally unstable and should naturally form photoionized clouds whenever the cooling time of hot halo gas is short compared to the age of the galaxy. This behaviour naturally leads to a two-phase model of gaseous galactic halos, where cool clouds can form in approximate pressure equilibrium with a hot medium and are produced in abundance within the cooling radius (Spitzer, 1956; Mo & Miralda-Escudé, 1996; Maller & Bullock, 2004). On the other hand, there is evidence at small radii pointing to important impacts of galactic winds on the MgII absorbers: the absorbers are not distributed symmetrically relative to the axes of galactic disks, but they tend to be closer to the minor axis (Bordoloi et al., 2011, 2012; Kacprzak et al., 2011, 2012; Lundgren et al., 2012). The distribution of MgII absorption systems around galaxies is therefore likely to be sensitive to processes involving both inflow and outflow of material into and from the regions containing the bulk of the stellar mass in galaxies.

The association of MgII absorbers with galaxies implies a large-scale cross-correlation of these objects. The cross-correlation is in general a result of two effects. First, if every galaxy is surrounded by a spherical gas halo, a MgII absorber located at an impact parameter  $r_p$  from a galaxy may be produced by gas clouds populating the halo of this galaxy. Second, the MgII absorber may be associated with a different galaxy that might be a satellite of the first, with halos that are in the process of merging, or might also be an unrelated galaxy in a separate halo that is spatially correlated with the first, following the usual galaxy autocorrelation. In the limit of impact parameters smaller than the typical size of a galaxy halo, the first effect dominates, while in the limit of large impact parameters the second effect is the important one. The total observed effect is a combination of the two over a wide range of intermediate impact parameters, and it is impossible to cleanly separate the two contributions. The non-linear regime is highly complex and depends on the way that MgII absorbers are distributed around galaxies within halos (e.g., Tinker & Chen, 2008). In the large-scale limit, the cross-correlation of MgII absorbers and galaxies should follow the form of the galaxy correlation function, with an amplitude that depends on the mean bias factor of the two populations, while for small scales the exact form of the cross-correlation depends on the physics that determine the distribution of MgII systems in galactic halos. Hence, measuring the large-scale clustering amplitude helps determine the halo population that the MgII absorbing clouds are associated with.

The large-scale MgII-galaxy cross-correlation was first measured using the photometric catalog of Luminous Red Galaxies in the Sloan Digital Sky Survey (hereafter, SDSS; see York et al., 2000) and the set of individually detected MgII absorbers in the spectra of SDSS quasars by Bouché et al. (2004), Bouché et al. (2006), Lundgren et al. (2009), Gauthier et al. (2009) and Lundgren et al. (2011). In the absence of precise galaxy redshifts, only

the projected cross-correlation function can be measured. The work by Lundgren et al. (2009), based on a set of 2705 MgII absorbers with rest-frame equivalent width  $W > 0.8 \text{ \AA}$  over the redshift interval  $0.36 < z < 0.8$ , found that the form of the projected cross-correlation is well matched by the Luminous Red Galaxy auto-correlation in the impact parameter range  $0.3 h^{-1} \text{Mpc} < r_p < 30 h^{-1} \text{Mpc}$ , and measured the bias factor of these MgII systems to be  $b_{\text{Mg}} = 1.10 \pm 0.24$ . Gauthier et al. (2009) performed a similar analysis for a sample of 1158 MgII absorbers with  $W < 1 \text{ \AA}$  over the redshift interval  $0.4 < z < 0.7$  and found the bias factor of these MgII systems to be  $b_{\text{Mg}} = 1.36 \pm 0.38$ . Both works found an indication that weak absorbers, with  $W < 1.5 \text{ \AA}$ , cluster more strongly (i.e., they have a larger bias factor) than strong absorbers, and are therefore located in more massive halos on average, although this result was not of high statistical significance. The method used by Bouché et al. (2006), Lundgren et al. (2009) and Gauthier et al. (2009), based on a catalog of identified MgII systems, requires careful attention to the selection function of *both* galaxies and MgII systems through an extensive use of simulations, because the number of absorbers will obviously be enhanced in regions of the survey containing more galaxies and more quasar spectra, or where the spectra are of higher signal-to-noise ratio, owing to variable observing conditions and also intrinsic clustering of the quasar sources.

We present a different approach in this paper to measure the cross-correlation of massive galaxies and MgII absorbers, based on the galaxies with spectroscopically-measured redshifts of the new Baryon Oscillation Spectroscopic Survey (hereafter, BOSS) of the SDSS-III Collaboration (Eisenstein et al., 2011; Dawson et al., 2013). Instead of identifying individual MgII absorbers, we use a stacking method to measure the average MgII absorption around a galaxy as a function of the impact parameter and redshift separation. In other words, we measure the redshift-space cross-correlation function of galaxies and MgII absorption. Our approach is similar to that of Zhu & Ménard (2013b), who have measured the mean CaII absorption around galaxies, and to Zhu et al. (2013), who have obtained a similar measurement of the large-scale MgII absorption; we compare their results with ours and discuss the differences near the end of this paper. The data set we use is described in Section 2, and the method is presented in detail in Sections 3 and 4. We present the results in Section 5, which are applied to infer the mean bias factor of MgII systems in Section 6. Finally we summarize our conclusions in Section 7. Throughout this paper we use the  $\Lambda$ CDM model with  $H_0 = 68 \text{ km s}^{-1} \text{ Mpc}^{-1}$  and  $\Omega_m = 0.3$ .

## 2. DATA SAMPLE

The first step in the analysis is to identify quasar-galaxy pairs in which the quasar sightline passes within a specified bin of projected radius, or impact parameter  $r_p$ , from the foreground galaxy. For the background quasar sample we use the quasar catalogue of Schneider et al. (2010) from the 7th Data Release (DR7, Abazajian et al., 2009) of the SDSS-II Collaboration (Gunn et al., 1998; York et al., 2000; Gunn et al., 2006; Eisenstein et al., 2011; Bolton et al., 2012; Smee et al., 2013), with 105,783 spectroscopically confirmed quasars. For the galaxies, the CMASS catalogue (Dawson et al., 2013) of the SDSS-III Collaboration that is prepared for the 11th Data Release (DR11, extension of the SDSS

DR9 (Ahn et al., 2012) and the SDSS DR10 (Ahn et al., 2013)) is used, which contains a total of 938,280 galaxies. The DR11 galaxies represent the majority of the final BOSS sample, also covering most of the sky area included in DR7. We exclude any galaxies at redshift lower than 0.35, corresponding to  $1 + z = \lambda_{min}/\lambda_{MgII}$ , where we set  $\lambda_{min} = 3800$  as the shortest wavelength with sufficient signal-to-noise ratio to provide a useful MgII absorption signal. This requirement reduces the galaxy sample to 895,472 galaxies. The quasar sample could be increased by including the DR11 sample from BOSS, but most of the new quasars in DR11 are fainter than those in DR7 (having therefore lower S/N) and are at a high redshift, at which the MgII lines associated with the CMASS galaxies appear superposed with the Ly $\alpha$  forest.

The mean MgII absorption around galaxies is computed by stacking all the spectra within a certain range of impact parameters from a galaxy. In general, all quasars probing a line-of-sight within a maximum proper impact parameter that was set to  $r_{p,max} = 12.8$  Mpc are included in the spectral stacking, provided that the following restrictions are met: first, in order to avoid broad absorption line systems associated with quasar outflows, the redshift of the quasar,  $z_q$ , must be larger than that of the galaxy,  $z_{gal}$ , by a minimum amount, corresponding to a velocity  $v = 0.04c$ ,

$$1 + z_q > R(1 + z_{gal}) , \quad (1)$$

where  $R = \sqrt{(1 + v/c)/(1 - v/c)} \simeq 1.041$ . Second, because the presence of the Ly $\alpha$  forest substantially increases the noise in quasar spectra, pairs where the galaxy MgII line would fall in the Ly $\alpha$  forest region of the quasar are also excluded; in other words, we require

$$(1 + z_{gal})\lambda_{MgII} > (1 + z_q)\lambda_{\alpha} , \quad (2)$$

where  $\lambda_{MgII} = 2798.743\text{\AA}$  is the mean wavelength of the MgII doublet, and the hydrogen Ly $\alpha$  wavelength is  $\lambda_{\alpha} = 1215.67\text{\AA}$  at the rest-frame. Note that the quasars that have been reported to have BALs are also included in the sample. We have tried removing them and we found that the measurements are not significantly changed. We believe that this is because we are only using small windows on the quasar spectra and therefore must not be including many of these BALs into the analysis.

The luminosity and redshift distributions of all the DR11 CMASS galaxies meeting these two conditions for at least one quasar that is within an impact parameter  $b_{max} = 12.8$  Mpc, as computed from the angular separation at the redshift of the galaxy, are shown in figure 1. Note that the density of quasars in DR7 implies that each galaxy has on average  $\sim 3$  quasars within this impact parameter, therefore the majority of galaxies have at least one quasar pair and these distributions are nearly the same as those of the whole DR11 CMASS sample. These distributions represent the characteristics of the galaxies for which we measure the mean MgII absorption equivalent width as a function of impact parameter in this paper.

### 3. STACKING PROCEDURE

This section describes the method we used to measure the average MgII absorption equivalent width as a function of impact parameter from the CMASS galaxies. In general,

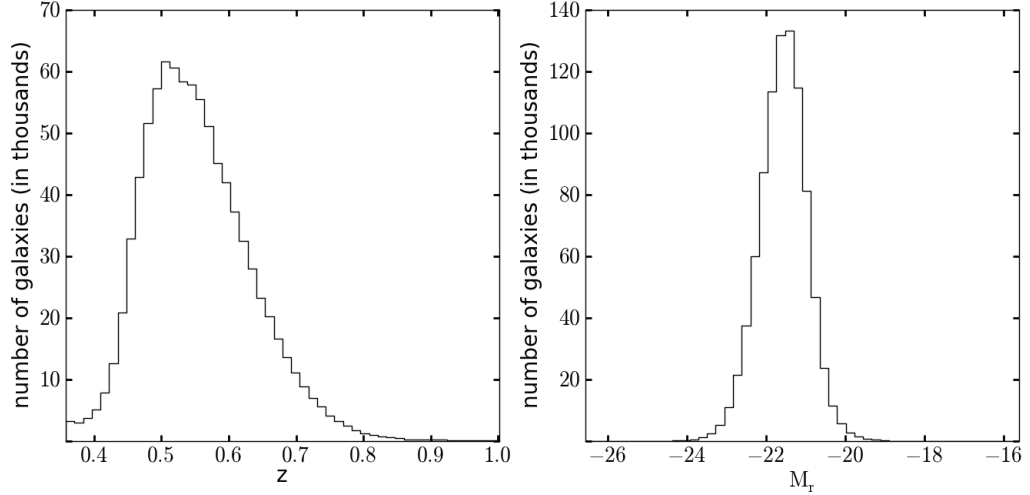


FIGURE 1. Redshift (left panel) and luminosity (right panel) distributions for the 895,472 selected CMASS galaxies (see texts for details).

the mean transmission fraction  $\bar{F}$  of light from a background quasar due to MgII absorption line systems can be written as a function of the impact parameter  $r_p$  and velocity separation  $v$  from a galaxy, as

$$\bar{F}(r_p, v) = \exp[-\tau_e(r_p, v)] = \exp[-\tau_{e0}(1 + \delta_{\text{Mg}}(r_p, v))] . \quad (3)$$

Here,  $\tau_e$  is the effective optical depth, and  $\tau_{e0}$  is its average value at any random position, irrespective of the presence of a galaxy. The perturbation  $\delta_{\text{Mg}}$  is the relative increase of the effective optical depth of MgII absorption associated with the presence of a galaxy at impact parameter  $r_p$  and velocity separation  $v$ . The shape of this perturbation as a function of  $v$ , for a given impact parameter, is rather complicated because it arises from the distribution of relative velocities of a set of doublet lines with different degrees of saturation; besides, the observations are affected by the instrumental resolution and the binning. We will return to these details later. The mean effective optical depth at a random position can be expressed in terms of the rest-frame equivalent width distribution of MgII absorbers, as

$$\tau_{e0} = \int_0^\infty dW \frac{\partial^2 \mathcal{N}}{\partial W \partial z} (1+z) \frac{W[1 + \bar{q}(W)]}{\lambda_{\text{MgII}}} , \quad (4)$$

where  $\lambda_{\text{MgII}} = 2798.743 \text{ \AA}$  is the mean wavelength of the MgII absorption line doublet, the equivalent width  $W$  is that of the strongest line of the doublet at  $\lambda = 2796.35 \text{ \AA}$ , and  $\bar{q}(W)$  is the mean equivalent width ratio of the two doublet lines.

Our aim in this paper is to measure the excess in the effective optical depth,

$$\delta\tau_e(r_p, v) = \tau_e(r_p, v) - \tau_{e0} = \tau_{e0}\delta_{\text{Mg}}(r_p, v) , \quad (5)$$

which is induced by the presence of a galaxy at impact parameter  $b$  and velocity separation  $v$ . This quantity is directly related to the cross-correlation of MgII clouds with CMASS galaxies. We will focus in particular on the projected value of  $\delta\tau_e$ , obtained after integration over velocity, and its relationship to the projected cross-correlation. The method we use to measure this cross-correlation is to average the transmitted fraction over a large number of lines-of-sight within a given range of impact parameter, in order to reduce the photon noise and the noise arising from quasar continuum variability.

A crucial step to measure the MgII-galaxy cross-correlation, in the form of  $\delta\tau_e$ , is to estimate the quasar continuum with a method that is, to the best possible degree, free of systematic errors when averaging over a large number of lines-of-sight. In particular, it is important to ensure that the presence of a MgII line itself, which in most cases may be too weak to be individually detected in the relatively low signal-to-noise ratio SDSS quasar spectra, does not bias the estimate of the continuum. Obviously, if the spectral region where we expect to find the MgII line associated with a galaxy is used for the continuum determination, the continuum estimate may be systematically biased too low because of the presence of an undetected MgII line. This systematic bias may be important when stacking large numbers of spectra, even though the MgII lines causing the bias are not individually detected in any single spectrum.

To illustrate the importance of the quasar continuum determination for the problem of measuring the average MgII absorption around galaxies at large impact parameters, we explore two different methods and we perform a number of tests for the presence of systematic errors. The first method, designated as *mean subtraction*, is specifically designed for our problem, while the second method, designated as *spline fitting*, is a standard spline fitting method that uses the entire spectrum to determine the continuum, including the region where the associated MgII line is expected, and is therefore subject to the systematic error described above. We now describe each method in detail. Tests of the methods that show that the mean subtraction method correctly recovers the mean equivalent width and the spline fitting method is subject to various systematic errors, including the continuum fitting bias mentioned above, are presented in Appendix A.

**3.1. Method 1: Mean subtraction.** The first approach uses the mean spectrum of all quasars as a continuum fit model. Each quasar spectrum is divided by the mean quasar spectrum, and then a linear fit to this ratio is obtained around the spectral region of the expected MgII line for each galaxy-quasar pair, but without using the narrower central interval where the MgII line should be located. This linear fit is used to further improve the continuum estimate, allowing for intrinsic variations of the quasar continua. The results are then stacked for all quasar-galaxy pairs at each interval of impact parameter, after shifting to the redshift of the galaxy in each pair, to obtain the final composite MgII absorption spectrum. We now explain each of these steps in detail.

**3.1.1. Generating the mean spectrum.** The mean quasar spectrum is generated using the DR7 quasar spectra following a similar approach as the one undertaken by Vanden Berk et al. (2001). The mean spectrum in Vanden Berk et al. (2001) was generated using 1,800 quasars (figure 3 of Vanden Berk et al., 2001), so our mean spectrum is more accurate

because of the much larger number of quasars available in DR7. In addition, we normalize the spectra using a spectral window that is particularly suited to obtaining the most accurate continuum model in the region where MgII absorption lines are found. There is therefore a small difference between our mean spectrum and that of Vanden Berk et al. (2001).

The quasar spectra are first shifted to the rest-frame, using the redshifts of Schneider et al. (2010), and rebinned into a common wavelength scale of 1 Å per bin, which is close to the resolution of the observed spectra when shifted to the rest frame. The values of the flux and the error at each pixel in the new binning are determined by the average values of the flux and error in the original pixels that are projected, partly or fully, to the new pixel, weighted by the fraction of the new bin covered by each original bin. Each quasar spectrum, denoted by an index  $j$ , is normalized with a normalizing factor  $n_j$  equal to the mean flux in the interval 2,000 – 2,600 Å,

$$n_j = \sum_i f_{ij}/N_j. \quad (6)$$

where  $f_{ij}$  is the measured flux value at pixel  $i$  of spectrum  $j$ , and  $N_j$  is the number of pixels in the rest-frame wavelength interval  $2,000 \text{ Å} < \lambda_{ij}(1+z_j) < 2,600 \text{ Å}$ . Any quasar spectra that do not cover this entire range of rest-frame wavelength are discarded. The final number of quasar spectra that are averaged in each 1 Å bin is shown in figure 2. The flat top corresponds to the spectral window used to compute the normalizing factor  $n_j$ . Note that the total number of quasar spectra used in this method is 70,650. The number of quasars shown in figure 2, roughly 68,600 quasars, is lower than the total number of spectra used because we removed the pixels affected by sky lines. For each sky line, we remove a set of neighboring pixels following the algorithm summarized in Palanque-Delabrouille et al. (2013) (for a more detailed explanation of the algorithm refer to Lee et al., 2013).

The rest-frame wavelength interval of 2000 – 2600 Å is also used to assign a mean signal-to-noise ratio  $s_j$  to each spectrum, calculated as

$$s_j = \frac{\sum_i f_{ij}/N_j}{\left(\sum_i e_{ij}^2/N_j\right)^{1/2}}, \quad (7)$$

where  $e_{ij}$  is the noise of the flux  $f_{ij}$ . The mean, normalized quasar spectrum is then obtained as a weighted average of all the quasar spectra,

$$\bar{f}_i = \frac{\sum_j w_j (f_{ij}/n_j)}{\sum_j w_j}, \quad (8)$$

where the weights  $w_j$  are set equal to

$$w_j = \frac{1}{s_j^{-2} + \sigma_I^2}. \quad (9)$$

The constant  $\sigma_I$  is introduced to avoid the highest signal-to-noise ratio spectra from excessively contributing to the final average, taking into account the presence of intrinsic quasar spectral variability, while reasonably weighting down the more noisy spectra. We fix this

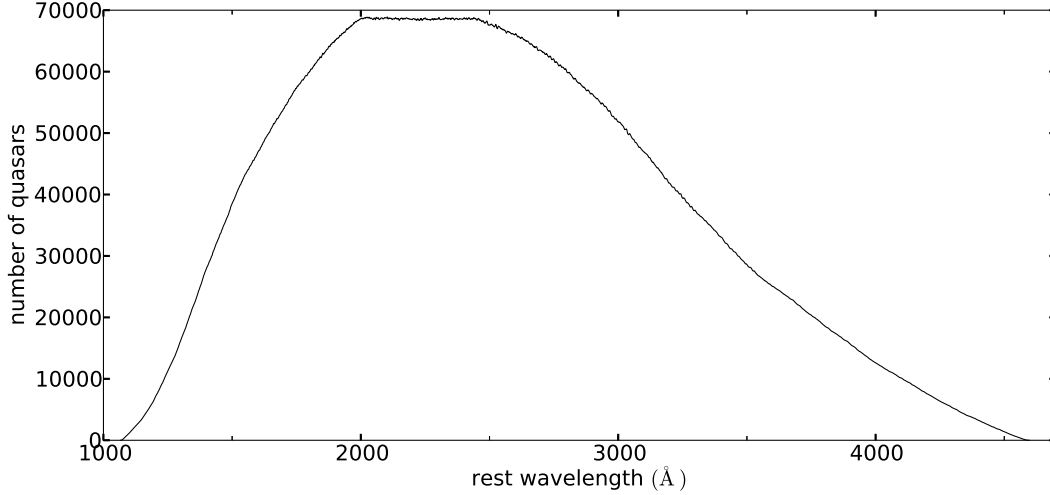


FIGURE 2. Number of quasar spectra contributing to each  $1 \text{ \AA}$  bin of the mean spectrum, as a function of rest-frame wavelength. The flat feature corresponds to the spectral range used to compute the normalizing factor  $n_j$ . Outside this range the number of quasars contributing to the mean quasar spectrum decreases because some of the quasar spectra do not extend to that wavelength. The flat top correspond to the spectral window used to compute the normalizing factor  $n_j$ . Outside this range the number of quasars contributing to the mean quasar spectrum decreases because some of the quasar spectra do not extend to that wavelength.

constant to  $\sigma_I = 0.05$  (a reasonable estimate for the typical fractional intrinsic variability) throughout this paper. The resulting mean spectrum is shown in figure 3.

**3.1.2. Generating the composite MgII absorption spectra.** The composite MgII absorption spectra are obtained by stacking the spectra of all the quasars having a galaxy within the corresponding impact parameter bin, after being shifted to the rest-frame of the galaxy in the region around the MgII doublet wavelength. For each quasar-galaxy pair, the quasar spectrum is first rebinned in a velocity variable  $v$ , defined in terms of the wavelength separation from the MgII absorption line in the rest-frame of the galaxy at redshift  $z_{gal}$ ,

$$v = c \cdot \frac{\lambda - \lambda_0}{\lambda_0}, \quad (10)$$

where  $\lambda_0 = \lambda_{MgII}(1 + z_{gal})$ , and  $\lambda_{MgII} = 2798.743 \text{ \AA}$ . We use the same linear rebinning method described in Section 3.1.1, with a bin size  $\Delta v = 50 \text{ km s}^{-1}$ . The mean spectrum is also rebinned in the same manner, but using  $\lambda_0 = \lambda_{MgII}(1 + z_{gal})/(1 + z_q)$ , where  $z_q$  is the quasar redshift, because the mean quasar spectrum is computed in the quasar rest-frame.

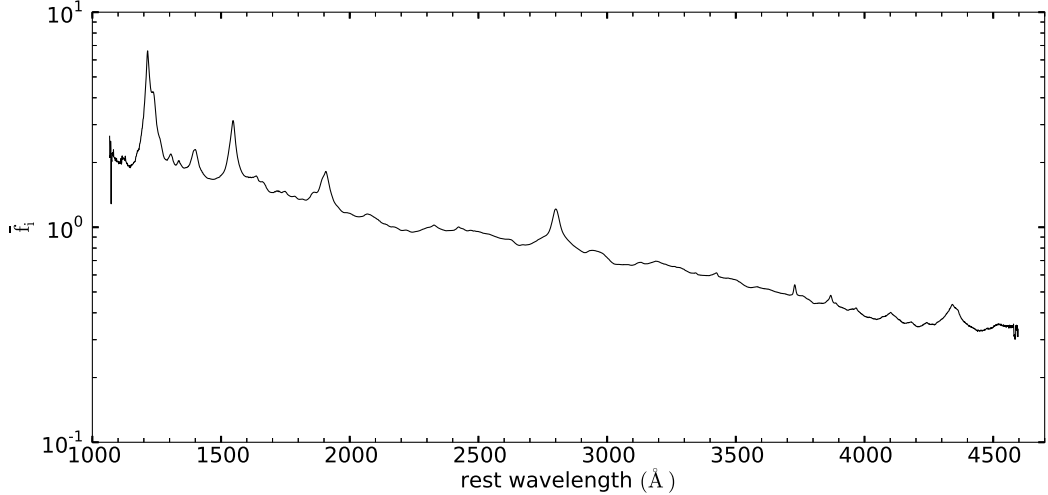


FIGURE 3. Mean spectrum of the weighted-average obtained from the 70,650 DR7 quasars, normalized in the rest-frame wavelength interval from 2000 to 2600 Å. This mean spectrum is used as a continuum model.

The rebinned spectra  $f_{ik}^{(r)}$ , where the  $i$  index now labels the new bins in  $\nu$ , and the  $k$  index labels each quasar-galaxy pair in a certain impact parameter bin, are then divided by the continuum to obtain a first estimate of the transmission fraction  $F_{ik}^{(0)}$ ,

$$F_{ik}^{(0)} = \frac{f_{ik}^{(r)}/n_{j(k)}}{\bar{f}_i}, \quad (11)$$

where the normalization factor  $n_j$  is that of the  $j$  quasar corresponding to each pair  $k$ . The mean quasar spectrum  $\bar{f}$  is understood to be the rebinned one and evaluated at the same bins in  $\nu$  for each quasar-galaxy pair. Hence, if all quasars had identical intrinsic emission spectra, and in the absence of intervening absorption and observational noise, this transmission would be equal to unity for all quasars. The errors are normalized in the same way and computed according to  $E_{ij} = e_{ij}/n_j/\bar{f}_i$ .

In order to account for intrinsic variations in the spectra of quasars, we allow for a local smooth gradient in the ratio of each quasar spectrum to the mean spectrum in the region around each expected MgII absorption line. This is modelled by first calculating a weighted average value of  $F^{(0)}$  on two intervals in  $\nu$  on each side of the expected MgII absorption associated with the galaxy, which are far enough from the center so that any associated absorption can be neglected. The intervals used throughout this paper are  $-5000 \text{ km s}^{-1} < \nu < -2000 \text{ km s}^{-1}$  and  $2000 \text{ km s}^{-1} < \nu < 5000 \text{ km s}^{-1}$ , with their weighted averages designated as  $F_k^{(-)}$  and  $F_k^{(+)}$ , respectively. The weights are set to  $w_{ik} = (\sigma_{n,ik}^2 + \sigma_I^2)^{-1}$ , where  $\sigma_{n,ik} = E_{ik}/F_k^{(+,-)}$  is the inverse signal-to-noise ratio at each pixel

(we use the averages  $F_k^{(+)}$  and  $F_k^{(-)}$  for the signal instead the values at each pixel  $F_{ik}^0$  in order to avoid biasing the result by systematically giving higher weights to pixels with positive noise). We use, as before,  $\sigma_I = 0.05$ . Weighted averages of the mean velocities  $v_k^{(-)}$  and  $v_k^{(+)}$  are computed in the same manner, which are usually close to the central values of the intervals ( $-3500$  and  $+3500 \text{ km s}^{-1}$ ), but not exactly so. A linear function  $L_{ik}$  matching these two points is then defined,

$$L_{ik} = F_k^{(-)} + (F_k^{(+)} - F_k^{(-}))(v_i - v_k^{(-)}) / (v_k^{(+)} - v_k^{(-)}) . \quad (12)$$

In order to better adjust the quasar continuum in the presence of unrelated random absorption lines or bad pixels, the calculation of the two weighted averages  $F_k^{(-)}$  and  $F_k^{(+)}$  is recomputed after eliminating all outlier pixels in which the normalized flux deviates by more than 3-sigma from the fitted linear function, i.e., pixels where  $\|F_{ik}^{(0)} - L_{ik}\| > 3(\sigma_{n,ik}^2 + \sigma_I^2)^{1/2}$ . If more than 20% of the pixels in any of the two intervals are rejected under this criterion, the quasar spectrum is considered anomalous in the region of the expected MgII line and the quasar-galaxy pair under consideration is rejected and not included in the final processing.

The transmission fraction is then corrected by this linear fit as

$$F_{ik} = F_{ik}^{(0)} + (1 - L_{ik}) . \quad (13)$$

We note here that although it would be in principle more correct to divide by the linear fit, setting  $F_{ik} = F_{ik}^{(0)} / L_{ik}$ , we found that this procedure inevitably introduces a systematic feature in the final stacked spectrum owing to the fact that a Gaussian error in the function  $L$  results in a non-gaussian distribution of the final transmission  $F$  when  $L$  is in the denominator, which is very difficult to correct for. We therefore decided to subtract  $L$  following equation (13). This means that the equivalent width of an individual absorber is overestimated by the average of the function  $L$  over the pixels of the absorber in our method, but we find that on average this factor is equal to unity to very high precision, as shown in the Appendix A, so that a correction is not necessary.

Finally, we use the same weights as in equation (9) to compute the final composite spectrum and its errors,

$$\bar{F}_i = \frac{\sum_k F_{ik} w_{j(k)}}{\sum_k w_{j(k)}} ; \quad \bar{E}_i^{-2} = \frac{\sum_k E_{ik}^{-2} w_{j(k)}}{\sum_j w_{j(k)}} . \quad (14)$$

The index  $j(k)$  refers to the quasar index  $j$  corresponding to each quasar-galaxy pair labeled by the index  $k$ . We exclude from this sum any pixel of any spectrum where the normalized flux  $F_{ik}$  is below  $-2$  or above  $+3$  in the interval from  $-5000$  to  $+5000 \text{ km s}^{-1}$ , as these values are considered excessively noisy or affected by bad pixels.

The whole procedure is illustrated in figure 4 with a couple of examples, one with an individually detected MgII absorption system and one without any individually detected MgII absorption but with a random metal absorption line. Note that the contribution of these random metal absorption lines is later corrected for (Section 3.3).

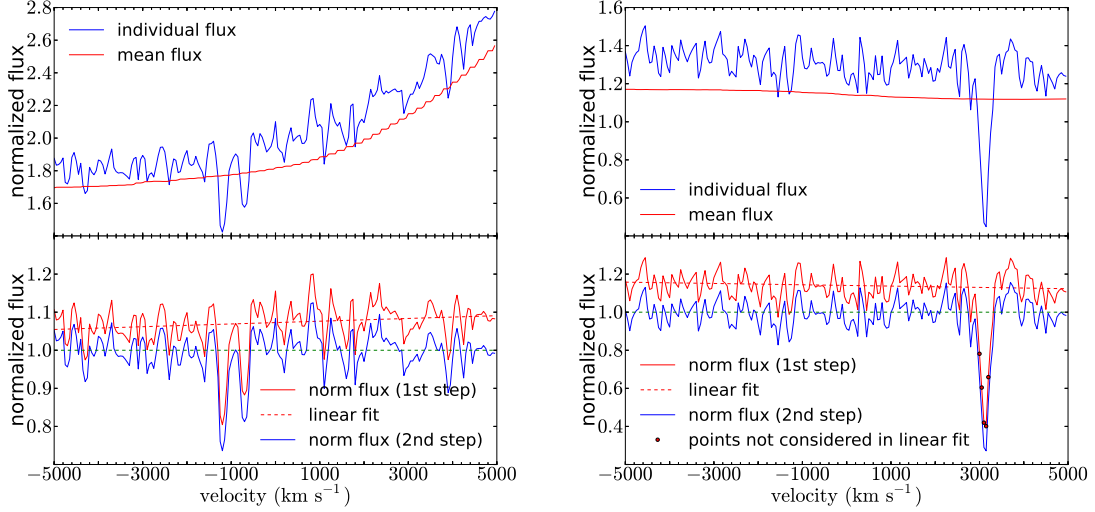


FIGURE 4. Examples illustrating the procedure explained in Section 3.1.2. The left column shows a case with a detected individual MgII absorption system, and the right column a case with no detectable associated MgII absorption system, but with an unrelated metal absorption line. The top panels show the normalized flux of the spectral region,  $f_{ik}^{(r)}/n_{j(k)}$  (blue line), and the normalized mean spectrum  $\bar{f}_i$  (red line). The bottom panels show the transmission  $F_{ik}^{(0)}$  (red solid line), the computed linear fit  $L_{ik}$  (red dashed line), and the corrected transmission  $F_{ik}$  (blue line). In the bottom right panel, the points indicate pixels that are excluded from the linear fit. A horizontal green dashed line at a transmission of 1 is included for visual aid.

**3.2. Method 2: Spline fitting.** As a second approach to determine the continuum, we use the method described in York et al. (2005), based on fitting a spline curve with an adjustable stepsize that is adapted to decrease in spectral regions of known quasar emission lines. The normalization of each quasar spectrum is done in this case by dividing the spectra by this continuum model,  $c_{ij}$ , both for the fluxes and errors:

$$F'_{ij} = f_{ij}/c_{ij} ; \quad E'_{ij} = e_{ij}/c_{ij} . \quad (15)$$

In the same way as for the first method, the normalized spectra are rebinned into the variable  $v$  with binwidth of  $50 \text{ km s}^{-1}$ . The final composite spectrum is calculated using the same weights as in equation (9),

$$\bar{F}'_i = \frac{\sum_k F'_{ik} w_{j(k)}}{\sum_k w_{j(k)}} ; \quad \bar{E}'_i{}^{-2} = \frac{\sum_k E'_{ik}{}^{-2} w_{j(k)}}{\sum_k w_{j(k)}} . \quad (16)$$

Chunk	Pairs	Chunk	Pairs	Chunk	Pairs	Chunk	Pairs
N-1	254304	N-6	254302	N-11	254307	N-16	254354
N-2	254229	N-7	254415	N-12	253259	N-17	254321
N-3	254407	N-8	254287	N-13	254290	N-18	254246
N-4	254357	N-9	254307	N-14	254369	N-19	254397
N-5	254261	N-10	254283	N-15	254395	N-20	254339
S-21	300 865	S-22	300 881				

TABLE 1. Number of quasar-galaxy pairs included in each of the 22 chunks.

**3.3. Unbiasing the composite spectra.** After the stacking of all the normalized spectra of quasar-galaxy pairs as a function of the velocity variable  $v$  has been completed by using either continuum fitting method, the mean value of the transmission  $\bar{F}_i$  that is obtained far from the expected MgII line (i.e., at large values of  $\|v\|$ ) is close to unity but not exactly so. The main reason for this is the presence of random metal absorption lines (unrelated to the galaxy of the pair) that are detected above a  $3\sigma$  fluctuation and therefore excluded when fitting the continuum. However, there may be other reasons affecting this mean background of  $\bar{F}_i$  related to systematic effects in the noise distribution and the continuum fitting method. We eliminate this bias by performing the same linear fit to the stacked spectrum as in Section 3.1.2, using again the velocity intervals  $(-5000, -2000)$  and  $(2000, 5000)$  km s<sup>-1</sup> to measure two average values of  $\bar{F}_i$ , and obtaining a linear fit based on two points at the center of these intervals. The final normalized stacked flux is found by dividing by this linear fit.

Our results will actually be shown, for convenience, in terms of the effective excess optical depth, defined according to  $\delta\tau_{e,i} = -\log \bar{F}_i$ , in figures 6 to 8.

**3.4. Bootstrap errors.** The errors computed from the known observational noise in the observed quasar spectra that are stacked are actually a lower limit to the true errors. In reality, the intrinsic variability of real quasar continua and of the associated MgII and other random metal absorption lines imply the presence of additional errors that are not taken into account and which are correlated among the pixels of the final stacks. We therefore compute bootstrap errors, which are generally used in our analysis and model fits in this paper.

To calculate these bootstrap errors, we have divided the area of the DR11 catalog in which our quasar-galaxy pairs are located into 22 chunks, as shown in figure 5. The chunks have been constructed to contain a similar number of detected quasar-galaxy pairs. The survey area is first split into the North/South galactic hemisphere portions. The North part is divided into five declination ranges with roughly the same number of pairs in each of them, and then each declination range is divided into four right ascension portions, creating 20 chunks. The South part is divided in right ascension into two chunks only, since it has fewer objects than the North part. Pairs are counted as belonging to the chunk that contains the quasar, irrespective of the galaxy position.

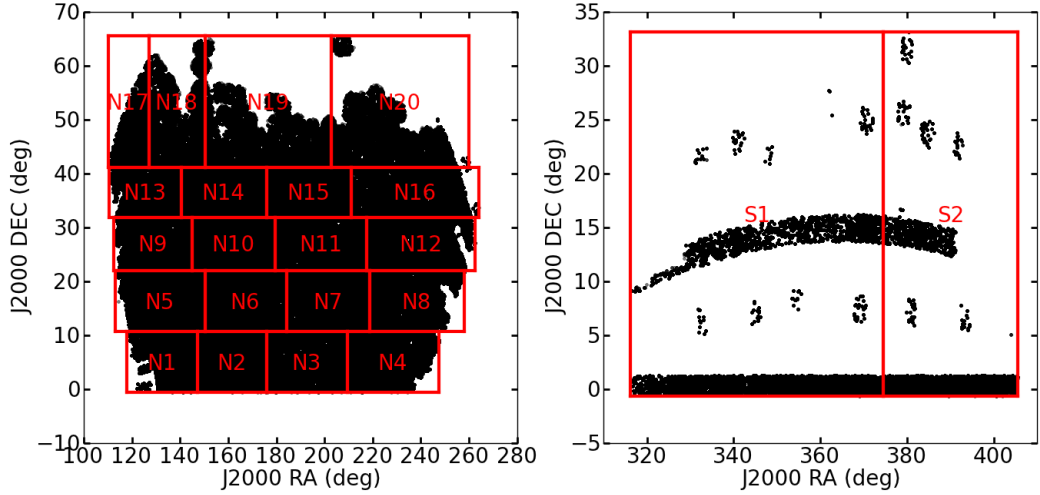


FIGURE 5. The 22 chunks in which the sample area is divided. Black dots, showing the quasar position of each quasar-galaxy pair, generate the black area where pairs are located.

Bootstrap errors are computed in the standard way, generating  $N = 1,000$  samples by randomly selecting 22 of the chunks with repetition, and then recalculating the composite spectra using both methods. Bootstrap errors are assigned to the final effective optical depth  $\tau_e$ , at each velocity bin and each impact parameter interval from the dispersion found among the 1,000 random samples. These bootstrap errors are computed for both continuum fitting methods.

We note that pairs near the chunk borders may have a galaxy that belongs to a different chunk than the quasar. This implies the presence of residual correlations because of the common galaxies in pairs belonging to different chunks, but we believe this effect is negligibly small because the most important error correlations should arise from the quasar spectra.

#### 4. MODEL FOR THE ABSORPTION PROFILE

Individual MgII absorption lines are usually fitted with Voigt profiles, with the equivalent width and the velocity dispersion as free parameters. Whenever the observed absorption profile is not adequately fitted in terms of the two Voigt profiles of the MgII doublet, one can include the presence of multiple cloud components with blended absorption lines in order to improve the fit. Here, we are analyzing a stack of a large number of MgII absorption systems that may be mostly undetected individually, but for which we can accurately predict the expected mean position from the redshift of the galaxy near the quasar line of sight. The effective optical depth in the stack,  $\tau_e = -\log(\bar{F})$ , should in this case have a single symmetric component for each line in the doublet, with a profile

reflecting the velocity dispersion of MgII absorbing clouds and galaxies in halos, as well as the large-scale halo correlation in redshift space for large impact parameters. For simplicity, we assume here a model with a Gaussian velocity distribution and a power-law form for the projected correlation function, as an approximation to the generally complex form of the galaxy-absorber cross-correlation function. This cross-correlation function can be modeled in terms of the Halo Occupation Distribution formalism (e.g. Gauthier et al., 2008; Zhu & Ménard, 2013a), but actually the distribution of MgII clouds in halos does not have to follow that of galaxies, and it will generally depend on complex physics of galaxy winds and gas accretion in the circumgalactic medium.

Our model has five free parameters. The first four are the central effective optical depth  $\tau_0$  of the strongest line in the doublet at a conventional normalization value of the impact parameter  $r_{p0}$  (set here to 1 Mpc), the power-law slope  $\alpha$  of the projected cross-correlation, the central velocity dispersion  $\sigma_0$ , and the mean equivalent width ratio  $q$  (where  $q = 1/2$  if all the absorption lines were unsaturated, and  $q = 1$  in the saturated case). We also include a variation of the velocity dispersion with radius, taking into account that in the limit of large radius, the Hubble expansion should lead to a linear increase of the effective dispersion. The fitted profile of the excess effective optical depth,  $\delta\tau_e(b, v)$  (as defined in equation 5), is

$$\delta\tau_e(r_p, v) = \frac{\tau_0}{\sqrt{1 + (xHr_p/\sigma_0)^2}} \left(\frac{r_p}{r_{p0}}\right)^{-\alpha} \left[ e^{-(v-v_1)^2/2\sigma^2} + q e^{-(v-v_2)^2/2\sigma^2} \right], \quad (17)$$

where

$$\sigma^2 = \sigma_0^2 + (xHr_p)^2. \quad (18)$$

The fifth model parameter is therefore the dimensionless constant  $x$ , which is the scale at which the velocity dispersion starts to increase compared to  $\sigma_0/H$ . Note that the parameter  $q$  is assumed to be independent of impact parameter, even though it should generally depend on it. In fact, at large impact parameter the mean saturation of the lines should decrease with impact parameter if the mean equivalent width also decreases, as indicated by observations (e.g. Gauthier et al., 2009; Chen et al., 2010a). Note also that the velocity dispersion includes the effect of the instrumental PSF (Smee et al., 2013) and finite spectral bin size in broadening the lines. Detailed modeling of these effects are neglected here to simplify the model. The origin of the velocity coordinate  $v$  is chosen by convention as the central position of the MgII doublet for an unsaturated line ( $q = 0.5$ ) at the redshift of the galaxy. Under this convention,  $v_1 = -256.05 \text{ km s}^{-1}$  and  $v_2 = 513.28 \text{ km s}^{-1}$ .

The fitting is performed by  $\chi^2$  minimization, computed including all the pixels of the stacked spectra in the central interval  $|v| < 2000 \text{ km s}^{-1}$ . Each pixel is weighted according to the bootstrap error measured in that pixel as described in Section 3.4, but without considering the cross-correlations of the errors between pixels. In practice, the bootstrap errorbars in different pixels of the stacked spectra are nearly equal. The spectrum outside the interval  $|v| < 2000 \text{ km s}^{-1}$ , which is used for deriving the continuum fit in Method 1, is not considered here for the fit. We note also that for a real Gaussian profile for each component of the MgII doublet, the continuum fitting of Method 1 implies that we formally

need to subtract a small constant from the double Gaussian in equation (17), equal to the integrated value of the model absorption over the interval  $v \in (2000, 5000) \text{ km s}^{-1}$  used for determining the continuum, but we neglect this effect here.

We use a Monte Carlo Markov Chain method to perform the  $\chi^2$  minimization to the five-parameter model fit. The errors of the parameters are also obtained by repeating the model fit with bootstrap realizations. The average integrated equivalent width as a function of impact parameter can be obtained directly by integrating the effective optical depth over the interval used to fit the model,

$$W_e(r_p) = \int_{-2000 \text{ km s}^{-1}}^{2000 \text{ km s}^{-1}} \delta\tau_e(r_p, v) dv . \quad (19)$$

This mean equivalent width can be compared to the value predicted by the best-fit model,

$$W_e(r_p) = \sqrt{2\pi} \tau_0 \sigma_0 (1 + q) \left( \frac{r_p}{r_{p0}} \right)^{-\alpha} = W_{e0} \left( \frac{r_p}{r_{p0}} \right)^{-\alpha} . \quad (20)$$

## 5. RESULTS

The results of the stacked absorption profiles are obtained for a total of 17 impact parameter intervals, measured in proper units at the redshift of the galaxy. The first interval is for  $r_p < 50 \text{ kpc}$ , and the other 16 intervals are  $2^{(i-1)/2} < (r_p/50 \text{ kpc}) < 2^{i/2}$ , for  $i = 1$  to 16, up to a maximum impact parameter of 12.8 Mpc. The stacked profiles are shown as the effective optical depth,  $\tau_e = -\log(\bar{F})$ , in figures 6, 7 and 8. Results are presented for our two continuum fitting methods, the mean subtraction method (thick, blue solid line) and the spline fitting method (thin red line). The errorbars plotted on the left side are the rms value of the bootstrap error of  $\tau_e$  in one pixel, which has little variation among different pixels in each stacked spectrum. The results of the fitted model parameters and their bootstrap errors described in Section 4 are given in table 2 (the cross-correlations of the parameter errors and are omitted). Note that the spectra have not been corrected for the instrumental PSF, and therefore the fitted value of  $\sigma_0$  represents the combination of the intrinsic velocity dispersion of the absorbers relative to the galaxies and the spectral resolution. An anomalous result seen in this table is the large difference on the bootstrap error of the velocity dispersion  $\sigma_0$  in the mean subtraction and spline fitting methods. We have found this to be due to a bimodal distribution of the solution for  $\sigma_0$  in the mean subtraction method, arising from the presence of two minima of the likelihood function that are interchanged depending on the bootstrap realization. This anomalous behavior of the velocity dispersion has not been found to have important effects on the rest of the fitted parameters.

A more simplified model imposing  $x = 0$  was also considered, but was discarded in regards to the high values obtained for the velocity dispersion. The origin of such a large value is found in the composite spectra at large impact parameter where Hubble expansion starts to be significant. Based on this result, the  $x = 0$  restriction was relaxed.

The stacks shown in figures 6, 7 and 8 clearly show a mean absorption profile for the presence of the MgII doublet line at the expected positions. The amplitude of the random

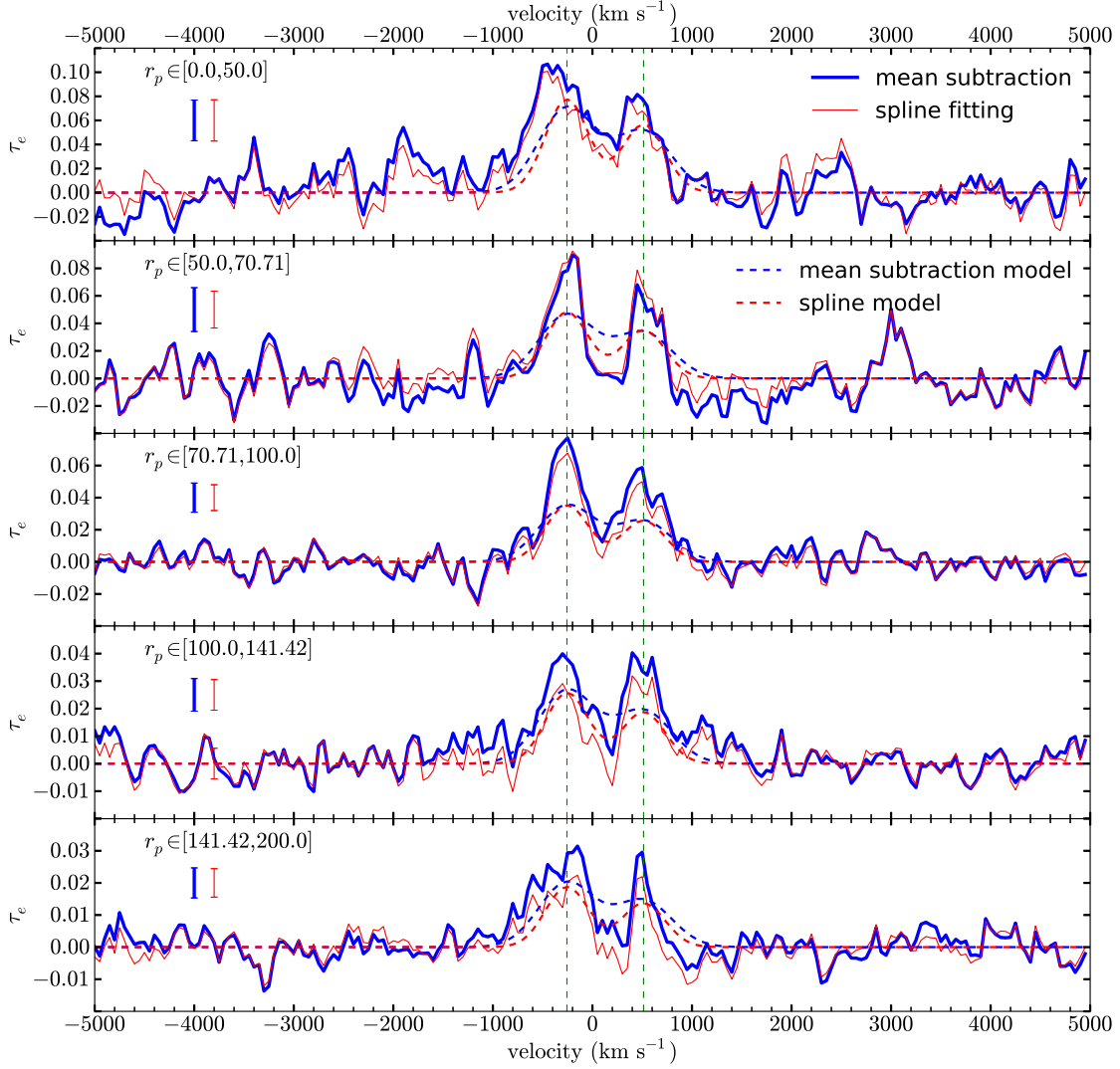


FIGURE 6. From top to bottom, composite spectra for increasing impact parameter intervals (in proper kpc). The effective optical depth is shown against velocity for the mean subtraction method (blue, thick solid line) and the spline fitting method (red line). The rms value of the bootstrap error in individual pixels is shown by the errorbars on the left. The blue, thick dashed line and the red dashed line are the best fit model (equation 17) for the mean subtraction and spline fitting methods respectively. A single set of parameters are fitted to all the 17 regions. Figures 7 and 8 show the spectra for the remaining impact parameter intervals. The stacks show a mean absorption profile for the presence of the MgII doublet line at the expected position. For visual guidance, green dashed lines mark the predicted position of the MgII doublet.

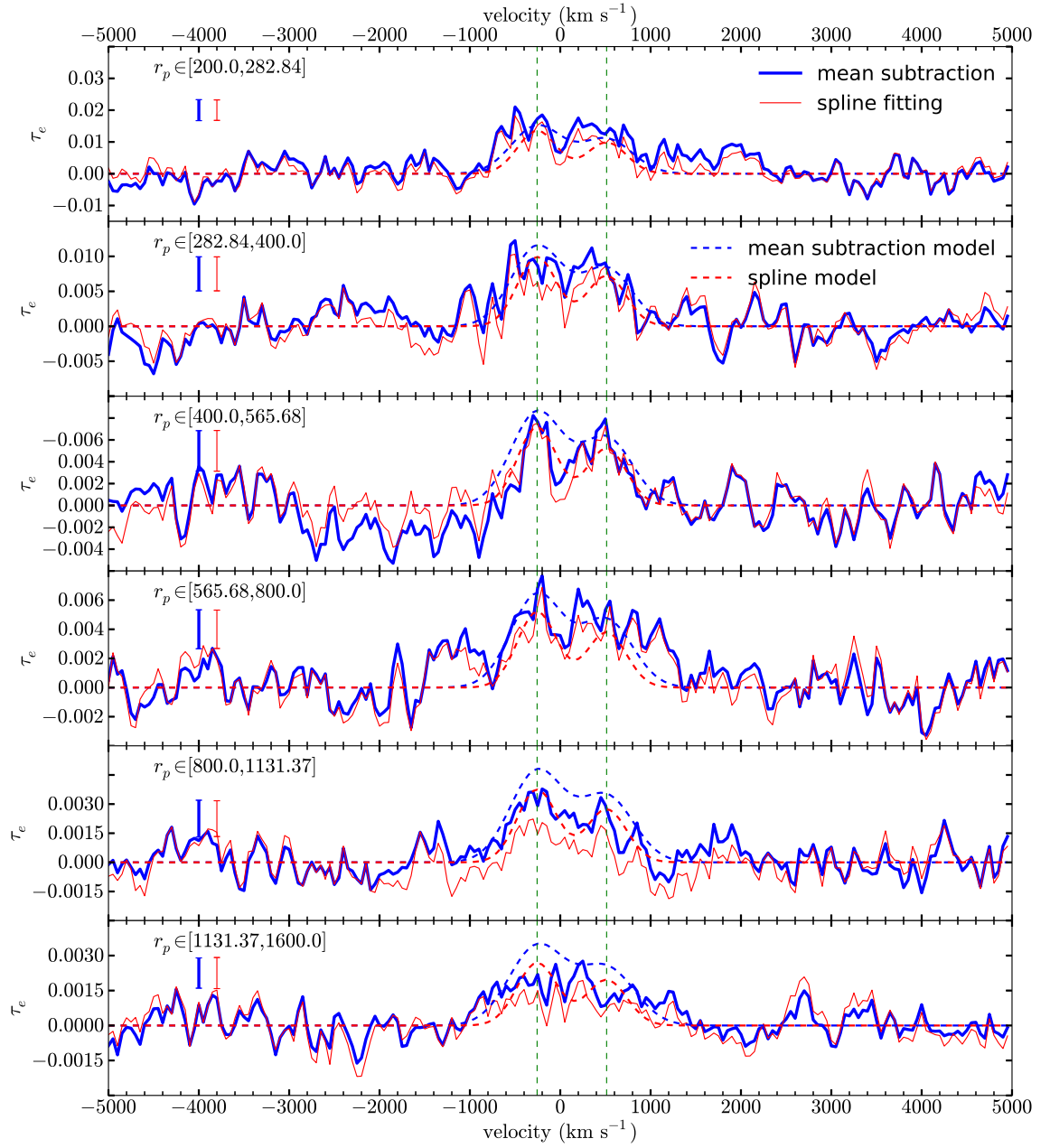


FIGURE 7. Continuation of figure 6.

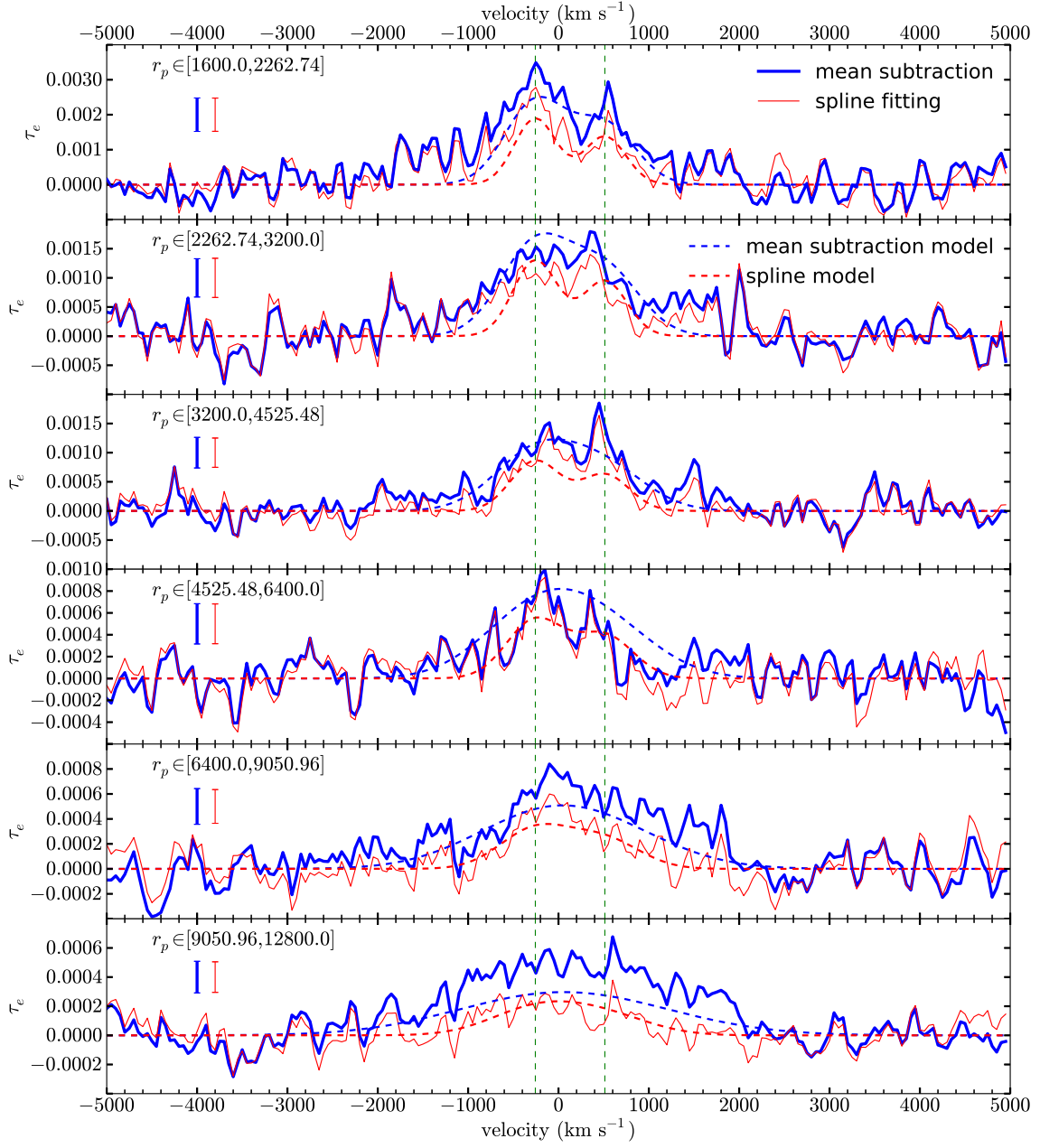


FIGURE 8. Continuation of figure 6.

	mean subtraction	spline fitting
$\tau_0$	$0.0048 \pm 0.0009$	$0.0037 \pm 0.0003$
$\alpha$	$0.81 \pm 0.07$	$0.91 \pm 0.07$
$\sigma_0 [\text{km s}^{-1}]$	$280 \pm 130$	$216 \pm 10$
$x$	$1.01 \pm 0.25$	$0.46 \pm 0.23$
$q$	$0.72 \pm 0.08$	$0.73 \pm 0.07$
$W_{e0} [\text{km s}^{-1}]$	$5.9 \pm 1.7$	$3.5 \pm 0.7$

TABLE 2. Best-fit values for the fitted parameters of the model described in Section 4 and shown as the lines in Figure 9. *First column:* Results using the mean subtraction method (see Section 3.1). *Second column:* Results using the spline method (see Section 3.2). Five independent parameters are fitted, and  $W_{e0}$  is related to the other parameters according to equation (20).

pixel-to-pixel variations outside of the central absorption feature is generally consistent with the computed bootstrap errorbars. The expected doublet feature of the MgII line is clearly present at small impact parameters, at  $r_p \lesssim 500$  kpc, and appears smoothed out at larger impact parameter. This effect is due an increasing velocity dispersion with impact parameter, which should approach a linear increase in the limit of large radius owing to the Hubble expansion. The fact that our parameter  $x$  is close to unity supports this interpretation, although we note that the precise expected theoretical value of  $x$  in the linear regime is not exactly one because of redshift distortions. We do not analyze this issue further in this paper because the maximum impact parameter that we analyze is not yet in the linear regime, and more detailed model predictions would be necessary for the velocity distribution of absorbers. We mention here that we initially considered a simpler model with  $x = 0$ , but this choice gave a substantially worse fit and resulted in a high value of the velocity dispersion because of the increase at large radius.

A value  $q \simeq 0.7$  is obtained for the line ratio of the MgII doublet, consistent with a mixture of saturated and unsaturated lines. It has been previously reported that the mean equivalent width of the MgII lines decreases with impact parameter (Gauthier et al., 2009, and references therein). This result may imply that absorbers are less saturated at larger impact parameters, and should therefore have a decreasing value of  $q$ , although this interpretation depends on whether the internal velocity dispersion of the absorbing clouds varies with impact parameter (note that this internal velocity dispersion is much smaller than the velocity dispersion of absorbing components around their host galaxies). Our model assumes a constant value of  $q$  for simplicity.

The mean equivalent widths obtained with our two methods, by directly integrating the effective optical depth in the stacked spectra as in equation (19), are shown in figure 9 as blue triangles for the mean subtraction method, and red squares for the spline fitting method. These values and their bootstrap errors are also given in table 3, together with the number of galaxy-quasar pairs that contribute to the stacked spectrum at each impact parameter bin. Note that this mean equivalent width is for the sum of the two lines in

the MgII doublet. There is a systematic difference in the mean equivalent width obtained with the two methods; the spline fitting method yields a systematically smaller equivalent width compared to the mean subtraction method, and the discrepancy increases with impact parameter, reaching a factor  $\sim 2$  at  $r_p = 10$  Mpc. As mentioned previously in Section 3, the reason for this difference is that the spline fitting method uses the spectral region where MgII absorption is expected to determine the continuum. The presence of weak lines that remain undetected in individual spectra causes the continuum to be underestimated in a way that depends on the signal-to-noise ratio and the equivalent width of the undetected line in a complex manner. This systematic underestimate of the continuum causes the underestimate of the mean equivalent width. Appendix A presents quantitative tests demonstrating the presence of this systematic error of the spline fitting method, and shows also that the result obtained with the mean subtraction method, which does not use the stacked spectrum in the region of the MgII absorption to determine the continuum, is free of any similar systematic effect to the extent that we are able to determine.

The green circles with errorbars in figure (19) show the results of Zhu et al. (2013), who have used a sample of galaxies and quasar spectra similar to ours to infer the same mean equivalent width as a function of impact parameter. Their result is systematically below ours, roughly by a factor  $\sim 2$  at all impact parameters, and is lower even compared to our spline fitting method. We believe the reason is again due to the systematic underestimate of the continuum. The continuum fitting method used by Zhu et al. (2013) also uses the observed spectra in the region where MgII absorption is expected in a rather complex way that is described in Zhu & Ménard (2013b), and the systematic error that this induces is difficult to predict but may in principle explain why it produces a systematically low estimate of the equivalent width. The errorbars of Zhu et al. (2013) are also smaller than ours, since their continuum fitting can better remove any features of the quasar spectrum that are superposed with the MgII absorption lines, at the cost of introducing a systematic bias in the continuum estimate.

## 6. DISCUSSION

**6.1. Relation of the mean equivalent width to the bias factor of MgII absorption systems.** Our measurement of the cross-correlation of MgII absorption systems and galaxies in the CMASS catalog of BOSS clearly reflects properties of the spatial distribution of these two objects. In the limit of large scales, when the fluctuations are in the linear regime, any population of objects that traces the large-scale mass perturbations is characterized by its bias factor (e.g. Cole & Kaiser, 1989), and the autocorrelation is equal to the correlation function of the mass times the square of the bias factor. The cross-correlation of two classes of objects is, in the same large-scale limit, equal to the mass correlation function times the product of the two bias factors. On small, non-linear scales, the correlations are more complex and they depend on other physics that determine the distribution of galaxies and MgII absorbers in relation to dark matter halos.

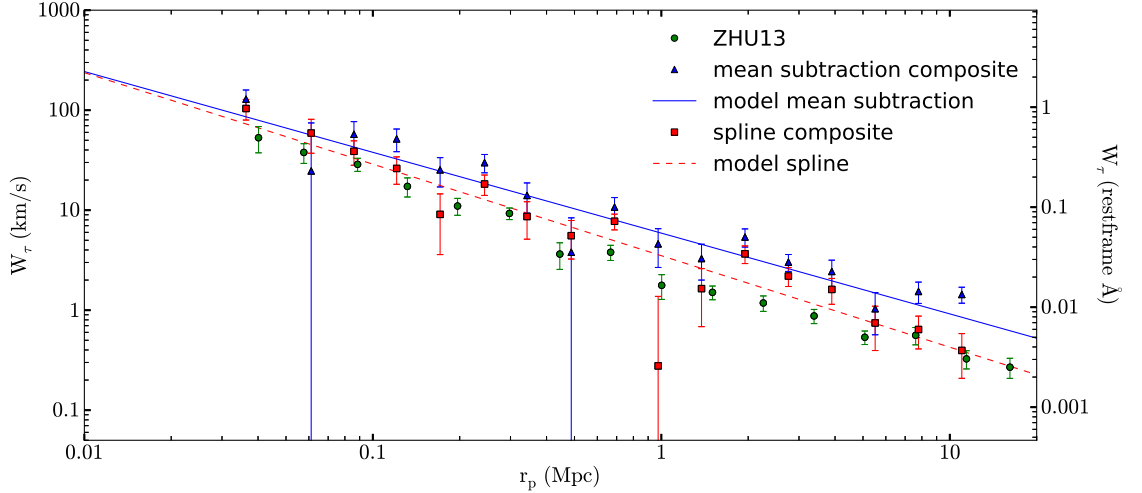


FIGURE 9. Measured rest-frame mean equivalent width  $W_e$  of the MgII doublet (shown in  $\text{km s}^{-1}$  and in  $\text{\AA}$ ), versus proper impact parameter. Blue triangles are obtained from the mean subtraction continuum method, and red squares use the spline fitting method. Errorbars have been obtained by the bootstrap method. Lines are the best-fit power-law model to the data for both methods. Green circles are the results of Zhu et al. (2013). Note that the results for the mean subtraction method are systematically higher than the rest. This is explored in further detail in the appendix A.

Our stacked spectra measure the mean excess of the effective optical depth as a function of impact parameter  $b$  and velocity separation  $v$  from a galaxy. This quantity is related to the mean MgII absorption perturbation,  $\delta_{\text{Mg}}(r_p, v)$ , as

$$\tau_e(r_p, v) = \tau_{e0} (1 + \delta_{\text{Mg}}(r_p, v)) \quad (21)$$

where  $\tau_{e0}$  is the mean MgII effective optical depth, defined in equation 4. This perturbation is equal to the cross-correlation function of MgII absorbers and galaxies, convolved with the mean doublet absorption profile of a MgII system, and is the function that is measured in our stacking results in figure 6. In practice, our interest is focused on the projected correlation function, related to the integrated absorption  $W_e(r_p)$  in equation (19). When the cross-correlation is integrated, the complications arising from the convolution with the mean doublet line profile and the spectrograph resolution are avoided.

Here, we shall make two approximations to physically interpret our measurement of  $W_e(r_p)$ : first, we neglect the effect of the finite integrating range  $\pm 2000 \text{ km s}^{-1}$  that we have used, ignoring the difference from integrating to infinity in the range of impact parameters we use. Second, we assume that the cross-correlation of MgII systems and CMASS galaxies is the same as the auto-correlation of CMASS galaxies times the ratio of bias factors  $b_{\text{Mg}}/b_g$

$r_p$ [kpc]	mean subtraction		spline fitting		$N_{pairs}$
	$\langle W \rangle$ [km s <sup>-1</sup> ]	$\sigma(\langle W \rangle)$ [km s <sup>-1</sup> ]	$\langle W \rangle$ [km s <sup>-1</sup> ]	$\sigma(\langle W \rangle)$ [km s <sup>-1</sup> ]	
(0, 50]	131.41	32.47	98.83	23.78	83
(50, 70.71]	25.03	48.37	60.12	22.05	105
(70.71, 100]	55.90	19.15	38.51	11.64	218
(100, 141.42]	52.07	12.28	25.59	7.73	444
(141.42, 200]	24.52	7.99	9.73	5.39	799
(200, 282.84]	28.97	5.81	17.10	4.29	1432
(282.84, 400]	15.42	4.72	8.57	3.46	2656
(400, 565.69]	2.94	4.05	4.95	2.06	4956
(565.69, 800]	11.08	2.42	7.41	1.37	9702
(800, 1131.37]	3.92	1.98	-0.05	1.10	19367
(1131.37, 1600]	3.02	1.29	1.59	0.96	38360
(1600, 2262.74]	5.42	1.09	3.45	0.72	76412
(2262.74, 3200]	2.97	0.56	2.07	0.49	150425
(3200, 4525.48]	2.45	0.66	1.60	0.43	293506
(4525.48, 6400]	1.15	0.47	0.80	0.35	565867
(6400, 9050.97]	1.46	0.36	0.66	0.22	1073597
(9050.97, 12800]	1.43	0.25	0.39	0.19	1981551

TABLE 3. Results on the mean equivalent width and errors shown in figure 9, presented here as a table. From left to right, impact parameter interval, mean rest-frame MgII equivalent width and its bootstrap error for the mean subtraction and spline fitting methods, and number of QSO-galaxy pairs used in the interval. The mean rest-frame equivalent widths are the sum of both lines in the doublet, in units of km/s (to obtain them in Angstroms they need to be multiplied by 0.00934).

of the two types of objects. In other words, we assume the linear relation can be extended into the non-linear regime as far as the ratio of the cross-correlation to the auto-correlation is concerned.

This assumption can be justified from observations of the correlations of galaxies of different luminosity. Zehavi et al. (2011) measured the projected correlation of galaxies in the DR7 catalogue in different luminosity ranges, and, to a good approximation, in the impact parameter range of our interest, the result is a fixed shape times the variable bias factor, as seen for example in their figure 6. The shape of the galaxy correlation can be interpreted as arising from the correlation among virialized halos and the distribution of galaxies within each halo (e.g. Zheng et al., 2005). This shape does vary slightly with luminosity, but the most important variation is the normalization determined by the bias factor. There is a greater variation of the shape of the projected correlation with galaxy color (see figure 21 in Zehavi et al., 2011). In addition, the projected cross-correlation

of galaxies of different color is not exactly equal to the geometric mean of the projected auto-correlations of the two types of galaxies (see their figure 15). Our assumption can only be considered as a first approximation that will need to be tested in the future, but it allows us to obtain a bias factor for MgII absorption systems assuming that they behave in a similar way as galaxies in the CMASS catalog.

This assumptions lead to the relation

$$W_e(r_p) = \tau_{e0} \int dv \delta_{\text{Mg}}(r_p, v) = \frac{\tau_{e0} H(z)}{1+z} \frac{b_{\text{Mg}}}{b_g} w_{gg}(r_p), \quad (22)$$

where  $w_{gg}(r_p)$  is the projected galaxy correlation function,  $b_g$  is the galaxy bias factor and  $b_{\text{Mg}}$  is the mean bias factor of MgII absorption systems, weighted in proportion to their equivalent width. We have used  $dv = H(z)/(1+z)dx$ , where  $dx$  is the comoving space coordinate that is integrated to obtain the projected galaxy correlation function, and  $z$  is the mean redshift of the galaxies and associated MgII absorption systems. This relation allows us to infer the bias factor of MgII systems empirically, using only the directly measured projected galaxy correlation. Its validity is strictly valid in the limit of large scales, but, as we shall see below, the ratio  $W_e(r_p)/w_{gg}(r_p)$  is roughly constant, making our assumption plausible as a first approximation.

**6.2. Mean absorption from MgII systems.** The value of  $\tau_{e0}$  must be independently known before we can use the measured mean excess of MgII absorption around galaxies to infer the bias factor of MgII systems. This parameter can be estimated from equation (4) using models of the equivalent width distribution that fit the observational data.

We use the double exponential model of Nestor et al. (2005),

$$\frac{\partial^2 \mathcal{N}}{\partial W \partial z} = \frac{N_{wk}^*}{W_{wk}^*} e^{-W/W_{wk}^*} + \frac{N_{str}^*}{W_{str}^*} e^{-W/W_{str}^*}, \quad (23)$$

where  $N_{str}^*$  and  $N_{wk}^*$  are the number of absorbers per unit of redshift in the strong and weak population, and  $W_{str}^*$  and  $W_{wk}^*$  are the characteristic rest-frame equivalent widths of the two exponential distributions. This model was fitted by Nestor et al. (2005) to their data, using mocks to correct for incompleteness at low equivalent widths. More recently, a compilation of high-resolution data was shown by Bernet et al. (2010) in their figure 5, reaching down to low equivalent widths. We include these observational results in figure 10, overplotting the fit that was obtained by Nestor et al. (2005), which has the following parameters:  $N_{wk}^* = 1.71 \pm 0.02$ ,  $W_{wk}^* = 0.072 \pm 0.001 \text{ \AA}$ ,  $N_{str}^* = 0.932 \pm 0.011$  and  $W_{str}^* = 0.771 \pm 0.014 \text{ \AA}$ . The observations are well reproduced by this fit, which we therefore use to compute  $\tau_{e0}$ .

Unfortunately, the sample of absorbers of Nestor et al. (2005) is somewhat heterogeneous, and the main uncertainty we encounter in using it to compute  $\tau_{e0}$  is due to the redshift evolution. A fit to this evolution was determined by Nestor et al. (2005), where the parameters of the exponential model vary as  $W^* \propto (1+z)^{0.634 \pm 0.097}$  and  $N^* \propto (1+z)^{0.226 \pm 0.170}$ , both for the weak and strong populations. We infer from their model fits and the mean value of  $N^*$  that the mean redshift of their sample is  $z \simeq 1.1$  and we use these

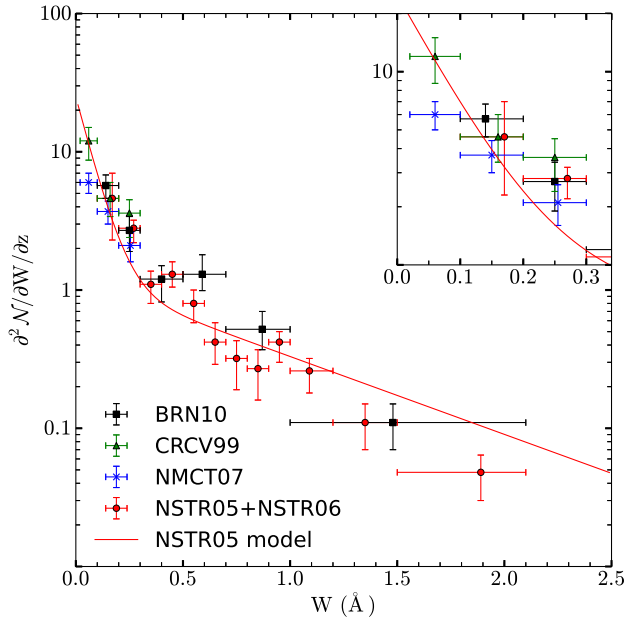


FIGURE 10. Rest-frame equivalent width distribution of MgII absorption systems. Data points are from Bernet et al. (2010) (black squares), Churchill et al. (1999) (green triangles), Narayanan et al. (2007) (blue crosses) and Nestor et al. (2005, 2006) (red circles). The overplotted solid line is the double exponential fit of Nestor et al. (2005) (see text). Top right panel is a zoomed view of the weakest absorption systems.

relations to convert the product  $N^*W^*$  to the mean redshift of the CMASS galaxy catalog,  $z \simeq 0.55$ . We find  $N_{str}^* W_{str}^* = 0.55 \text{ \AA}$  and  $N_{wk}^* W_{wk}^* = 0.095 \text{ \AA}$ , with an error that is close to 10%, although it is poorly defined because the errors in the redshift evolution of  $N_{str,wk}^*$  and  $W_{str,wk}^*$  should be correlated, and this information (and the exact redshift distribution of the absorbers) was not provided in Nestor et al. (2005).

From equation 4, we derive the value of  $\tau_{e0}$  in the double exponential model of equation 23,

$$\tau_{e0} = \frac{1+z}{\lambda_{\text{MgII}}} (1 + \bar{q}) (N_{wk}^* W_{wk}^* + N_{str}^* W_{str}^*) . \quad (24)$$

which yields a value  $\tau_{e0}(z = 0.55) = 6.5 \times 10^{-4}$ , with an error of about 10% but which is subject to uncertainties owing to the redshift evolution, the accuracy of the fit to the equivalent width distribution, and the value of  $\bar{q}$ . Our results will be given in terms of  $\tau_{e0}$  without including its error, with the understanding that this quantity will need to be better determined in the future from studies of the field population of MgII absorbers.

**6.3. Derivation of the bias factor of MgII systems.** We now use equation 22 to infer the bias factor of the MgII systems, as

$$b_{\text{Mg}} = b_g \frac{W_e(r_p)(1+z)}{w_{gg}(r_p)\tau_{e0}H(z)}. \quad (25)$$

Note that the factor  $(1+z)/H(z)$  appears because of our convention that the effective equivalent width  $W_e$  is measured in  $\text{km s}^{-1}$ , whereas  $w_{gg}$  is assumed to have been transformed to comoving length units. Instead of fitting our MgII-galaxy cross-correlation measurement with a power-law dependence with impact parameter (as in equation 17), we can directly fit the functional form that is determined from the observed projected galaxy correlation function, assuming that the shape is the same. To do this, we use the projected galaxy autocorrelation function obtained in Nuza et al. (2013) from the BOSS DR9 catalog of CMASS galaxies, and their prediction for the galaxy correlation function based on assigning galaxies to halos and subhalos in their MultiDark simulation. The measurements of Nuza et al. (2013) are represented as black points with errorbars in figure 11, and their model is shown as the black solid line (given in their figure 6 and table B1; note that we have corrected for the different cosmological model they use, with a present matter density  $\Omega_m = 0.27$  instead of our value  $\Omega_m = 0.3$ ). The blue points with errorbars are our measurements of  $W_e(r_p)r_p$  given in figure 9 and table 3, multiplied by the factor  $(1+z)/H(z)/\tau_{e0}$  to transform it into a projected cross-correlation, in units of  $\text{Mpc}^2$ . The galaxy bias factor obtained by Nuza et al. (2013) from this measurement is  $b_g = 2.00 \pm 0.07$ . This value is lower than that obtained by Guo et al. (2013),  $b_g = 2.16 \pm 0.01$ , for the average CMASS galaxy. Using the value given by Guo et al. (2013) would lead to a larger measured value of the bias factor of the MgII systems. As explained in Guo et al. (2013), the value of the galaxy bias increases with luminosity and redshift, and it can also depend on the range of scales used to fit its value. Here we use the galaxy bias value and the projected galaxy autocorrelation function of Nuza et al. (2013), but the discrepancy with the higher value obtained by Guo et al. (2013) needs to be resolved to remove this source of uncertainty on the derived bias value of the MgII absorption systems.

We now redo the fit to the measured  $\delta\tau_e(r_p, v)$  profiles presented in section 5, after replacing equation (17) by

$$\delta\tau_e(r_p, v) = \frac{b_{\text{Mg}} \tau_{e0}}{b_g \sqrt{2\pi}(1+q)} \frac{w_{gg}(r_p)H(z)}{(1+z)\sqrt{\sigma_0^2 + (xHr_p)^2}} \left[ e^{-(v-v_1)^2/2\sigma^2} + q e^{-(v-v_2)^2/2\sigma^2} \right]. \quad (26)$$

That is to say, we replace the power-law dependence of  $W_e$  on impact parameter by the model to the observed  $w_{gg}$  of Nuza et al. (2013). All the parameters except for  $b_{\text{Mg}}$  are kept fixed to the best fit obtained in section 5, and a new fit is obtained by matching only  $b_{\text{Mg}}$ . The function  $w_{gg}(r_p)$  is computed at our impact parameter bins by linear interpolation of the values of the model of Nuza et al. (2013). The result we obtain for the MgII absorption bias factor is

$$b_{\text{Mg}} = 1.50 \pm 0.19, \quad (27)$$

and the resulting fit for  $W_e(r_p)r_p$  is shown as the blue line in figure 11 (this blue line is simply the rebinned black line shifted by the factor  $b_{\text{Mg}}/b_g$ ). The error on this bias factor

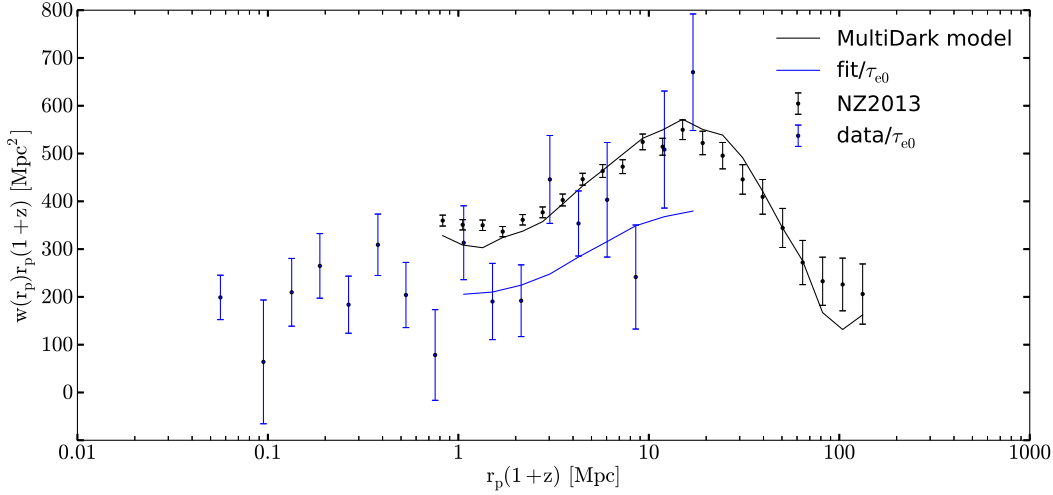


FIGURE 11. Projected correlation functions multiplied by the comoving impact parameter as a function of the comoving impact parameter  $r_p(1+z)$ . Black points with errorbars show the auto-correlation of CMASS galaxies from Nuza et al. (2013), and the blue ones are the mean equivalent width  $W_e(r_p)$  times the factor  $(1+z)/H(z)/\tau_{e0}$  (equal to the cross-correlation of MgII systems and CMASS galaxies), times  $r_p(1+z)$ . The black line is the MultiDark model prediction described in Nuza et al. (2013), and the blue one is the fit to  $W_e$ . The ratio of the two lines is the ratio of bias factors,  $b_{\text{Mg}}/b_g$ .

includes only the uncertainty of the fit that assumes the bootstrap errors in our stacked spectra, and does not include the error of  $\tau_{e0}$ , assumed to be  $\tau_{e0} = 6.5 \times 10^{-4}$ .

This value of the bias factor is consistent with that measured by Gauthier et al. (2009),  $b_{\text{Mg}} = 1.36 \pm 0.38$ , and also at with that measured by Lundgren et al. (2009),  $b_{\text{Mg}} = 1.10 \pm 0.24$ , at the  $\sim 1.5\sigma$  level. The galaxies that have a bias factor of 1.50 at  $z \simeq 0.5$  have a luminosity  $L/L_* \simeq 1$  (see Coupon et al., 2012; Marulli et al., 2013; Skibba et al., 2013; Guo et al., 2013; Arnalte-Mur et al., 2013). This result suggests that most of the MgII absorption systems are associated with typical  $L_*$  galaxies. However, our measurement of the bias factor remains subject to systematic uncertainties that will need to be improved; if the value of the bias is lowered to near unity, then the majority of MgII absorption systems could arise in the halos of galaxies of very low luminosity. Also both Lundgren et al. (2009) and Gauthier et al. (2009) find that weak absorbers tend to cluster more strongly than strong ones, although these conclusions were not of high statistical significance. This result, if confirmed, might provide a partial explanation for the discrepancy between our measurement for the bias factor and that of Lundgren et al. (2009).

Our measurement of the bias factor, and the implication on the types of galaxies associated with MgII systems, is of a different nature from previous measurements, which generally attempted to identify individual absorption systems and associate them with the nearest galaxy that can be identified in their vicinity above some luminosity threshold. In general, the association with an individual galaxy may be ambiguous when there are several galaxies in the vicinity of an absorber. In addition, galaxies of low luminosity that are found to be associated with a MgII absorber may have a larger bias factor than the average one for that luminosity, if they are found on denser environments than average.

We can compare our the results for the MgII-galaxy cross-correlation with those of Zhu et al. (2013). The modeling of Zhu et al. (2013) involves a free parameter, which they designate as  $f_{\text{MgII}}$ , that reflects the gas-to-mass ratio in halos (ignoring the degree of saturation of the absorption lines). Zhu et al. (2013) do not relate this parameter to the mean absorption of the field population of MgII absorbers, so they fit the amplitude of the cross-correlation with this unconstrained, free parameter. They determine a characteristic host halo mass for the MgII absorbers of  $M_h \simeq 10^{13.5} M_\odot$  based on the presence of a feature in the shape of the cross-correlation at  $r_p \sim 1$  Mpc that reflects a transition from the 1-halo term to the 2-halo term in their modeling. The weakness of this feature implies a poor determination of this characteristic halo mass (see the contours in their figure 6, showing the large degeneracy with the  $f_{\text{MgII}}$  parameter). We believe there are other problems with this methodology: the MgII absorbers are likely hosted in halos with a very wide mass range, which should cause a smoothing of any feature due to the transition from the 1-halo to the 2-halo term. In addition, the model assumes a specific density profile for the distribution of absorbers in halos that has not been tested and is not theoretically well motivated. In practice, the MgII absorbers are a new population of objects that can be distributed differently from any galaxies, which depends on the physics of gas cooling and galactic winds in a halos and is not predictable from simple models. Auto-correlations and cross-correlations of galaxies of different types have been found to have widely different shapes (see, e.g., figures 15 and 16 in Zehavi et al., 2011) which do not always possess the clear feature that is predicted for the correlation of dark matter halos of a specific mass. Therefore, our view is that there is insufficient evidence for the presence of any feature in the MgII-galaxy cross-correlation that may be used to determine a characteristic host halo mass.

Instead, we propose that the *amplitude* of this cross-correlation should not be fitted with a free parameter, but should be related to the field population (e.g., through the effective optical depth  $\tau_{e0}$  that we have introduced), and can then be used to determine the mean bias factor  $b_{\text{MgII}}$ , which should be equal to the mean bias factor of the host halos of the absorbers (weighted by their rest-frame equivalent width), and is robustly defined even if the range of host halo masses is very broad.

**6.4. The ratio of MgII-absorbing gas to the total mass.** Measurements of the average MgII absorption around galaxies can be compared with mass measurements averaged in the same way obtained from weak gravitational lensing. This comparison was done in Zhu et al. (2013) to obtain an estimate for the ratio of gas mass to total mass in the halos

around the CMASS galaxies of the BOSS survey. We now examine this question to point out a number of uncertainties in this derivation.

In general, the total column density of MgII in an individual absorber,  $N_{\text{MgII}}$ , is related to its integrated optical depth according to

$$N_{\text{MgII}} = \frac{m_e c^2}{\pi e^2} \frac{W_\tau}{f \lambda_{\text{MgII}}^2} = 1.13 \times 10^{20} \frac{W_\tau \text{ \AA}}{f \lambda_{\text{MgII}}^2} \text{ cm}^{-2} . \quad (28)$$

where  $e$  and  $m_e$  are the electric charge and mass of the electron, and  $f = 0.921$  is the total oscillator strength of the MgII doublet. The integrated optical depth is

$$W_\tau = \int d\lambda \tau(\lambda) , \quad (29)$$

where the integration is performed over a wavelength range that includes the entire absorption profile. However, the only quantity that is observed is the equivalent width,

$$W = \int d\lambda [1 - e^{-\tau(\lambda)}] . \quad (30)$$

When the optical depth of the absorber is much less than unity over the whole wavelength range, the absorber is unsaturated and  $W_\tau \simeq W$ . Otherwise, the column density is not directly measurable simply from the equivalent width. We now define an average saturation level for the population of absorbers,  $\bar{S}$ , as

$$\bar{S} = \frac{\int dW (\partial^2 \mathcal{N} / \partial W \partial z) W_\tau}{\int dW (\partial^2 \mathcal{N} / \partial W \partial z) W} . \quad (31)$$

Defining also  $x_{\text{MgII}}$  as the fraction of magnesium atoms in the absorbing gas that are in the MgII ionized species,  $g_{\text{Mg}}$  as the fraction of magnesium in the absorbers that is in the gas phase (as opposed to dust grains), and  $Z_{\text{Mg}}$  as the magnesium mass fraction compared to that of the Sun (we use a solar magnesium abundance by mass of  $7.0 \times 10^{-4}$ , and a magnesium mass  $m_{\text{Mg}} = 4.07 \times 10^{-23}$  g), we obtain that the total gas mass surface density in the MgII absorbers is

$$\Sigma_g(r_p) = (9.15 \times 10^{-7}) \frac{\bar{S}}{x_{\text{MgII}} g_{\text{Mg}} Z_{\text{Mg}}} \frac{W_e(r_p)}{\text{\AA}} \text{ g cm}^{-2} . \quad (32)$$

The total mass surface density around a CMASS galaxy in the BOSS sample has also been measured using weak gravitational lensing. We can therefore obtain the ratio of gas in MgII absorbers to the total mass by combining the two observational measurements. We use the recent measurement by Miyatake et al. (2013) based on weak lensing measurements in the CFHTLenS survey area. As an example, we compute the gas-to-mass ratio at a comoving projected radius of  $r_p(1+z) = 3$  Mpc. The differential surface density measured by Miyatake et al. (2013) at this radius is  $\Delta\Sigma = \bar{\Sigma} - \Sigma \simeq 2 M_\odot \text{ pc}^{-2}$  (see their figure 7). Near this radius,  $\Delta\Sigma(r_p)$  is falling with radius roughly as  $r_p^{-1}$ , so the mean surface density within  $r_p$  is  $\bar{\Sigma} \simeq 2\Sigma$ , and we can therefore use  $\Sigma \simeq \Delta\Sigma$ . At this same radius,  $W_e \simeq 0.03 \text{ \AA}$ , and substituting this value in equation (32), it produces  $\Sigma_g / \Sigma \simeq 8 \times 10^{-5} \bar{S} / (x_{\text{MgII}} g_{\text{Mg}} Z_{\text{Mg}})$ .

Using the mean ratio of baryons to total matter in the universe of  $\Omega_b/\Omega_m = 0.17$ , the fraction of baryons in the MgII absorbing gas would be  $\Sigma_g/\Sigma_b \simeq 5 \times 10^{-4} \bar{S}/(x_{\text{MgII}} g_{\text{Mg}} Z_{\text{Mg}})$ .

Therefore, the fraction of baryons in the MgII clouds can be a small one even if the mean metallicity is relatively low. However, the mean saturation parameter  $\bar{S}$  is likely much larger than unity, so it is possible that the MgII absorbers account for an important fraction of the baryons in galactic halos, and for the accreting material that fuels the star formation rate. We note that any further comparison of the detailed radial profiles of  $W_e(r_p)$  and  $w_{gg}(r_p)$  cannot be reliably used to infer a profile of the gas-to-mass ratio, because  $Z_{\text{Mg}}$  is likely to vary with  $r_p$ , since the heavy elements must have originated from galactic winds, and the values of  $\bar{S}$ ,  $x_{\text{MgII}}$  and  $g_{\text{Mg}}$  may also vary substantially with  $r_p$ . The mean value of the gas-to-mass ratio is still highly uncertain because of the unknown value of  $\bar{S}/(x_{\text{MgII}} g_{\text{Mg}} Z_{\text{Mg}})$ .

## 7. SUMMARY AND CONCLUSIONS

In this paper we have used the MgII line to measure the cross-correlation of MgII absorption and galaxies in BOSS. The large size of the samples we use (SDSS DR7 quasar catalog as background sample and DR11 CMASS galaxy catalog as foreground sample) enables a statistical approach to detect MgII absorption that is too weak to be detected individually and would otherwise be missed. We present a method to estimate the quasar continuum designed for this type of measurements and compare our results with those obtained by a more typical continuum estimate. Our main results can be summarized as follows:

- The method to fit the quasar continuum is crucial to measure the mean MgII equivalent width as a function of impact parameter. Methods that use the observed flux in the region near the galaxy redshift where the correlated MgII absorption is expected suffer from a systematic bias, because the absorption from individually undetected systems inevitably lowers the continuum estimate, causing an underestimate of the mean absorption. The tests presented in the Appendix A show that our mean subtraction method does not suffer from any systematic effect.
- We find that the cross-correlation of MgII absorption and CMASS galaxies follows the shape of the CMASS galaxies auto-correlation at large scales. We use the CMASS auto-correlation model from Nuza et al. (2013) and the measured galaxy bias factor to derive a bias factor of MgII absorbers of  $b_{\text{Mg}} = 1.50 \pm 0.19$ . This value is consistent with that measured by Gauthier et al. (2009),  $b_{\text{Mg}} = 1.36 \pm 0.38$ , and also with that measured by Lundgren et al. (2009) at the  $\sim 1.5\sigma$  level. It is possible that there is a real difference between the two bias factors because our measurement includes a contribution from weak MgII absorption systems, which may be more strongly clustered than the strong absorbers, but more accurate measurements will be necessary to clarify this question.

## ACKNOWLEDGMENTS

Funding for SDSS-III has been provided by the Alfred P. Sloan Foundation, the Participating Institutions, the National Science Foundation, and the U.S. Department of Energy Office of Science. The SDSS-III web site is <http://www.sdss3.org/>. IP and JM have been supported in part by Spanish grants AYA2009-09745 and AYA2012-33938.

SDSS-III is managed by the Astrophysical Research Consortium for the Participating Institutions of the SDSS-III Collaboration including the University of Arizona, the Brazilian Participation Group, Brookhaven National Laboratory, University of Cambridge, Carnegie Mellon University, University of Florida, the French Participation Group, the German Participation Group, Harvard University, the Instituto de Astrofísica de Canarias, the Michigan State/Notre Dame/JINA Participation Group, Johns Hopkins University, Lawrence Berkeley National Laboratory, Max Planck Institute for Astrophysics, Max Planck Institute for Extraterrestrial Physics, New Mexico State University, New York University, Ohio State University, Pennsylvania State University, University of Portsmouth, Princeton University, the Spanish Participation Group, University of Tokyo, University of Utah, Vanderbilt University, University of Virginia, University of Washington, and Yale University.

## REFERENCES

- Abazajian, K. N., Adelman-McCarthy, J. K., Agüeros, M. A., et al. 2009, *ApJS*, 182, 543  
Ahn, C. P., Alexandroff, R., Allende Prieto, C., et al. 2012, *ApJS*, 203, 21  
—. 2013, ArXiv e-prints, arXiv:1307.7735  
Arnalte-Mur, P., Martínez, V. J., Norberg, P., et al. 2013, ArXiv e-prints, arXiv:1311.3280  
Bahcall, J. N. 1975, *ApJL*, 200, L1  
Bahcall, J. N., & Spitzer, Jr., L. 1969, *ApJL*, 156, L63  
Bergeron, J., & Boissé, P. 1991, *A&A*, 243, 344  
Bergeron, J., & Stasińska, G. 1986, *A&A*, 169, 1  
Bernet, M. L., Miniati, F., & Lilly, S. J. 2010, *ApJ*, 711, 380  
Bolton, A. S., Schlegel, D. J., Aubourg, É., et al. 2012, *AJ*, 144, 144  
Bordoloi, R., Lilly, S. J., Kacprzak, G. G., & Churchill, C. W. 2012, ArXiv e-prints, arXiv:1211.3774  
Bordoloi, R., Lilly, S. J., Knobel, C., et al. 2011, *ApJ*, 743, 10  
Bouché, N., Murphy, M. T., & Péroux, C. 2004, *MNRAS*, 354, L25  
Bouché, N., Murphy, M. T., Péroux, C., Csabai, I., & Wild, V. 2006, *MNRAS*, 371, 495  
Chen, H.-W., Helsby, J. E., Gauthier, J.-R., et al. 2010a, *ApJ*, 714, 1521  
Chen, H.-W., Wild, V., Tinker, J. L., et al. 2010b, *ApJL*, 724, L176  
Churchill, C. W., Mellon, R. R., Charlton, J. C., et al. 2000, *ApJ*, 543, 577  
Churchill, C. W., Rigby, J. R., Charlton, J. C., & Vogt, S. S. 1999, *ApJS*, 120, 51  
Cole, S., & Kaiser, N. 1989, *MNRAS*, 237, 1127  
Coupon, J., Kilbinger, M., McCracken, H. J., et al. 2012, *A&A*, 542, A5  
Dawson, K. S., Schlegel, D. J., Ahn, C. P., et al. 2013, *AJ*, 145, 10  
Eisenstein, D. J., Weinberg, D. H., Agol, E., et al. 2011, *AJ*, 142, 72  
Gauthier, J.-R., Chen, H.-W., & Tinker, J. L. 2009, *ApJ*, 702, 50

- Gauthier, J.-R., Tinker, J., & Chen, H.-W. 2008, in COSPAR Meeting, Vol. 37, 37th COSPAR Scientific Assembly, 980
- Gunn, J. E., Carr, M., Rockosi, C., et al. 1998, *AJ*, 116, 3040
- Gunn, J. E., Siegmund, W. A., Mannery, E. J., et al. 2006, *AJ*, 131, 2332
- Guo, H., Zehavi, I., Zheng, Z., et al. 2013, *ApJ*, 767, 122
- Kacprzak, G. G., Churchill, C. W., Evans, J. L., Murphy, M. T., & Steidel, C. C. 2011, *MNRAS*, 416, 3118
- Kacprzak, G. G., Churchill, C. W., & Nielsen, N. M. 2012, *ApJL*, 760, L7
- Lanzetta, K. M., & Bowen, D. 1990, *ApJ*, 357, 321
- Lee, K.-G., Bailey, S., Bartsch, L. E., et al. 2013, *AJ*, 145, 69
- Lundgren, B. F., Wake, D. A., Padmanabhan, N., Coil, A., & York, D. G. 2011, *MNRAS*, 417, 304
- Lundgren, B. F., Brunner, R. J., York, D. G., et al. 2009, *ApJ*, 698, 819
- Lundgren, B. F., Brammer, G., van Dokkum, P., et al. 2012, *ApJ*, 760, 49
- Maller, A. H., & Bullock, J. S. 2004, *MNRAS*, 355, 694
- Marulli, F., Bolzonella, M., Branchini, E., et al. 2013, *A&A*, 557, A17
- Miyatake, H., More, S., Mandelbaum, R., et al. 2013, ArXiv e-prints, arXiv:1311.1480
- Mo, H. J., & Miralda-Escudé, J. 1996, *ApJ*, 469, 589
- Narayanan, A., Misawa, T., Charlton, J. C., & Kim, T.-S. 2007, *ApJ*, 660, 1093
- Nestor, D. B., Turnshek, D. A., & Rao, S. M. 2005, *ApJ*, 628, 637
- . 2006, *ApJ*, 643, 75
- Nuza, S. E., Sánchez, A. G., Prada, F., et al. 2013, *MNRAS*, 432, 743
- Palanque-Delabrouille, N., Yèche, C., Borde, A., et al. 2013, *A&A*, 559, A85
- Rao, S. M., Turnshek, D. A., & Nestor, D. B. 2006, *ApJ*, 636, 610
- Sargent, W. L. W., Young, P. J., Boksenberg, A., Carswell, R. F., & Whelan, J. A. J. 1979, *ApJ*, 230, 49
- Schneider, D. P., Richards, G. T., Hall, P. B., et al. 2010, *AJ*, 139, 2360
- Skibba, R. A., Smith, M. S. M., Coil, A. L., et al. 2013, ArXiv e-prints, arXiv:1310.1093
- Smee, S. A., Gunn, J. E., Uomoto, A., et al. 2013, *AJ*, 146, 32
- Spitzer, Jr., L. 1956, *ApJ*, 124, 20
- Steidel, C. C. 1995, in *QSO Absorption Lines*, ed. G. Meylan, 139
- Steidel, C. C., Dickinson, M., & Persson, S. E. 1994, *ApJL*, 437, L75
- Tinker, J. L., & Chen, H.-W. 2008, *ApJ*, 679, 1218
- Vanden Berk, D. E., Richards, G. T., Bauer, A., et al. 2001, *AJ*, 122, 549
- York, D. G., Adelman, J., Anderson, Jr., J. E., et al. 2000, *AJ*, 120, 1579
- York, D. G., Vanden Berk, D., Richards, G. T., et al. 2005, in *IAU Colloq. 199: Probing Galaxies through Quasar Absorption Lines*, ed. P. Williams, C.-G. Shu, & B. Menard, 58–64
- Zehavi, I., Zheng, Z., Weinberg, D. H., et al. 2011, *ApJ*, 736, 59
- Zheng, Z., Berlind, A. A., Weinberg, D. H., et al. 2005, *ApJ*, 633, 791
- Zhu, G., & Ménard, B. 2013a, *ApJ*, 773, 16
- . 2013b, *ApJ*, 770, 130
- Zhu, G., Ménard, B., Bizyaev, D., et al. 2013, ArXiv e-prints, arXiv:1309.7660

## APPENDIX A. TESTS OF THE CONTINUUM FITTING METHODS

The method to fit the quasar continuum is a crucial part of the measurement of the mean MgII absorption equivalent width as a function of impact parameter from a galaxy,  $W_\tau(b)$ , presented in this paper. The two methods we have used produce a different result, which is also different from the result reported by Zhu et al. (2013). It is therefore important to perform tests of these methods that can reveal the presence of systematic errors in the  $W_\tau(b)$  estimates. This appendix presents the results of three tests. The first one (section A.1) checks for any systematic mean absorption that might be artificially introduced by the continuum fitting method when there is no correlation between MgII absorbers and galaxies. The second one (section A.2) verifies that the correct equivalent width of an artificially introduced absorber in a spectrum is correctly recovered. Finally, section A.3 reveals the effect on the fitted continuum of the presence of weak absorbers that are individually undetected, and the way these absorbers can bias the estimate of the mean equivalent width.

**A.1. Systematic errors in the absence of correlations.** One might suspect that a small average absorption (either positive or negative) is artificially introduced by the method to fit the continuum, even when the regions selected to search for absorbers are completely random and should therefore have no average absorption. This might happen if the quasar continuum is systematically overestimated or underestimated, depending in a complex manner on the varying noise properties and the shape of the true quasar continuum. To test for this possibility, we have remeasured the mean MgII equivalent widths after rotating the right ascension coordinate of all the quasar by 10 degrees, in the two possible directions. The separation of 10 degrees is large enough to make any residual cross-correlation of galaxies and MgII absorbers completely negligible, so the measured correlation should be consistent with zero. Note that this procedure ensures that the auto-correlations that are present among the MgII absorbers, quasars and galaxies are preserved, so their contribution to the measurement errors of the cross-correlation is the same.

The result of this test is shown in figure 12, in the left panel for the mean subtraction method and the right panel for the spline fitting method. The real data set is shown as red circles with errorbars, after dividing by the best-fit power-law model that is described in Section 4 and plotted in figure 9. The two mock data sets (for each direction of the rotation in right ascension) are shown also after dividing by the same model, as black triangles and blue squares. In the absence of any systematics, the mean absorption in the mock data sets is expected to be zero, whereas the real data should produce a ratio to the best-fit model that is consistent with one. The results do not show any systematic errors for the mean subtraction method. There appears to be a small negative systematic absorption that is introduced by the spline fitting method, as indicated by the negative values of the mock sample in the right panel, at large impact parameters (where the mean equivalent width can be measured with the smallest errorbar). This average negative absorption is approximately equal to the best-fit model prediction at  $\sim 10$  Mpc, or  $\sim 0.3 \text{ km s}^{-1}$  (see figure 9). This result may be due to some subtle effect in the spline fitting method that introduces a small bias by systematically underestimating the continuum in the absence

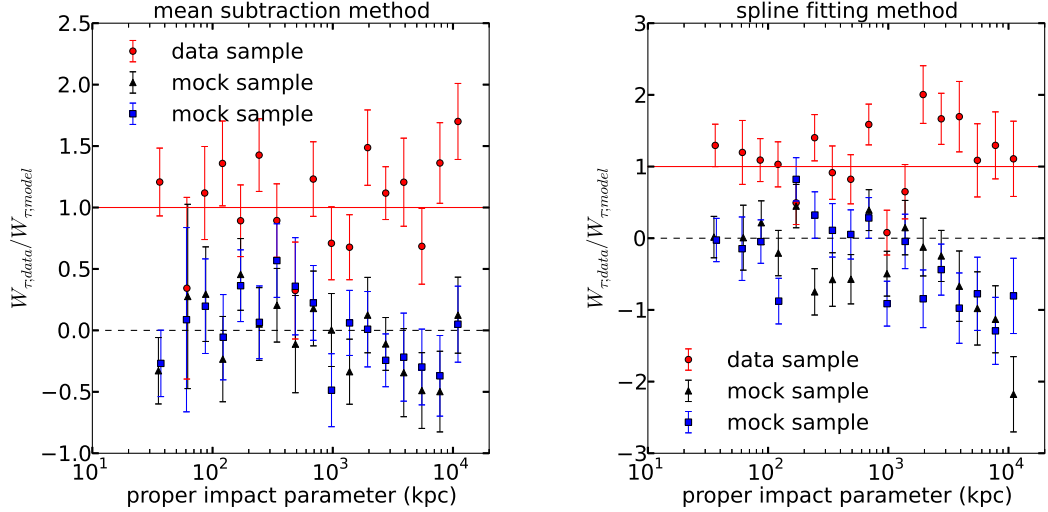


FIGURE 12. Ratio of the mean equivalent width in stacked spectra to the best-fit power-law model prediction, for the real data sample (red circles), and for a mock sample modified by rotating the quasar positions by 10 degrees in right ascension, in both directions (black triangles and blue squares). Errorbars are computed with the bootstrap method. This ratio should be consistent with zero for the mock sample in the absence of systematic errors, and with unity for the real data if the power-law model provides a good fit to the data.

of real absorption lines, possibly due to occasional false identifications of noise spikes as real absorbers. As we shall see below, the spline fitting method is actually affected by a more serious systematic error that partially eliminates the contribution of weak absorption systems to the mean equivalent width.

**A.2. Tests of the equivalent width measurement for individually detected systems.** We now test that the mean equivalent width measured for absorbing systems that are individually clearly detected above the noise agrees with other well established methods. For this purpose, we use the MgII absorber catalogue of Zhu & Ménard (2013b), which contains 35,752 absorption systems from the SDSS DR7 quasar spectra sample. The integrated equivalent widths we obtain for systems in this catalogue, using our two methods of mean subtraction and spline fitting, are compared with the equivalent widths provided in the catalogue in figure 13. There is a large scatter in the equivalent widths obtained with different methods. This result is not surprising, because the noise can change the determination of the continuum in random ways in different methods. In particular, in the method of the mean subtraction, the equivalent width is obtained by integrating the absorbed fraction over a wide interval around the absorber, according to equation (19), adding noise to the estimate. However, the average of the equivalent width estimator in

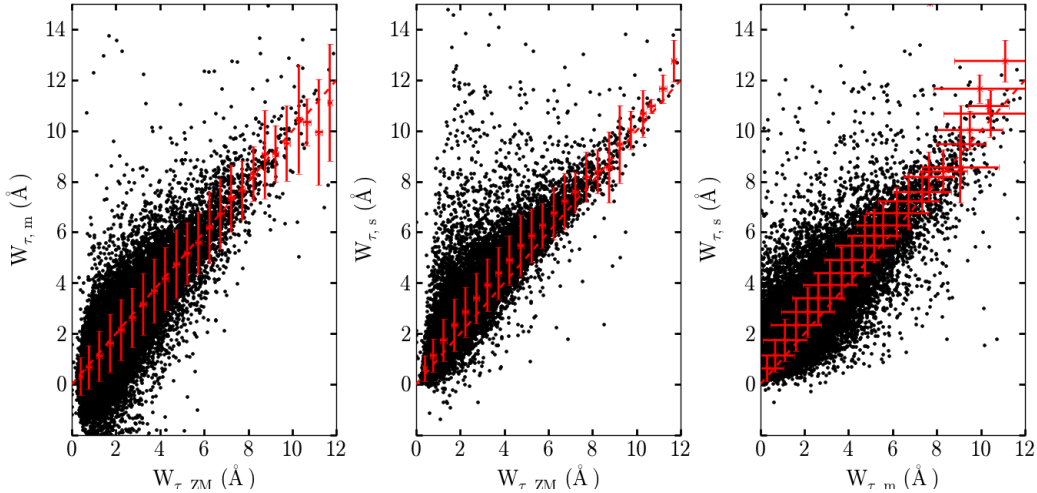


FIGURE 13. Comparison of the equivalent width estimates from different methods (see Section 3). From left to right, equivalent widths measured using the mean subtraction method,  $W_m$ , versus the value of the Zhu & Ménard catalogue,  $W_{ZM}$ ; spline fitting method value,  $W_s$ , versus  $W_{ZM}$ ; and  $W_s$  versus  $W_m$ . Red points are the average values in bins of  $\Delta W = 0.5 \text{ \AA}$  in the horizontal axis, with the dispersion in each bin indicated by the errorbars. One-to-one correspondence is marked by the red dashed line for visual guidance.

our mean subtraction method, shown by the red points in figure 13 (with an rms dispersion indicated by the errorbars), agrees very well with the equivalent width provided by the Zhu & Ménard (2013b) catalogue. The spline fitting method apparently suffers from a bias causing a 10 to 20% increase of the average of the equivalent width (see red points in middle panel of figure 13), which may be due to a tendency of this method to overestimate the continuum level around detected absorption lines.

### A.3. Impact of individually undetected systems on the mean equivalent width.

We now test how the presence of weak absorption systems that cannot be individually detected in a single spectrum but contribute to the mean equivalent width as a function of impact parameter from a galaxy can bias the estimate of the quasar continuum in the different methods we use. For this purpose, artificial absorbers are introduced in a spectrum, and then we refit the continuum and measure the change in the measured equivalent width.

As illustrative example, we have selected a set of 10 random quasar spectra. We then introduced absorbers at 10 random redshift values and computed the average values for the recovered width. The absorbers are inserted with a double Gaussian profile in the optical

depth, as expected for the MgII doublet,

$$\tau(v) = \frac{W_0}{\sqrt{2\pi}\sigma} \left( \frac{2}{3} e^{-(v-v_1)^2/2\sigma^2} + \frac{1}{3} e^{-(v-v_2)^2/2\sigma^2} \right), \quad (33)$$

where  $W_0$  is the total equivalent width of the doublet and  $\sigma$  is velocity dispersion. The zero velocity is conventionally chosen to be the central position of the MgII line for an unsaturated line, so that  $v_1 = -256.05 \text{ km s}^{-1}$  and  $v_2 = 513.28 \text{ km s}^{-1}$ . In the absence of any inserted absorber, the continuum determined in this spectrum is  $c(v)$ , the flux is  $f(v)$ , and the transmitted fraction is  $F(v) = f(v)/c(v)$ . This results in a certain value of the integrated equivalent width  $W$  measured over the interval  $-2000 \text{ km s}^{-1} < v < 2000 \text{ km s}^{-1}$ , by integrating  $F(v)$  over this range. To insert the absorber, the spectral flux is modified according to

$$f'(v) = f(v) - c(v) \left[ 1 - e^{-\tau(v)} \right]. \quad (34)$$

Then, a new continuum  $c'(v)$  is determined with the new flux, and a new transmitted fraction  $F'(v) = f'(v)/c'(v)$  is derived. Finally, the new equivalent width  $W'$  is determined by integrating  $F'$  over the same velocity interval.

The change in equivalent width caused by the insertion of an absorber,  $\Delta W = W' - W$ , is plotted in figure 14 as a function of the equivalent width  $W_i$  of the inserted absorber, obtained by integrating  $1 - \exp[-\tau(v)]$  over the same velocity interval that is used for determining  $W$  and  $W'$  ( $W_i$  is nearly equal to  $W_0$  in equation 33, except that the integrating interval does not extend to infinity). The different lines correspond to different values of the absorber velocity dispersion,  $\sigma$ . The blue lines represent the mean subtraction method, and they coincide precisely with  $\Delta W = W_i$  for all values of  $\sigma$ . The result, as expected, is that the continuum determined by this method is unaffected by the presence of the absorbers that have narrow widths compared to the chosen integrating interval width of  $4000 \text{ km s}^{-1}$ . The reason is that, in the mean subtraction method, the continuum  $c'(v)$  is determined using only the measured flux outside of this interval.

On the other hand, the spline fitting method (red lines in figure 14) is strongly biased to lowering the estimated continuum in response to the presence of a weak absorption system. The result is that the change caused by the absorber in the estimated equivalent width,  $\Delta W$ , can be much less than the true value, and the difference is a complex function of the equivalent width  $W_0$ , the velocity dispersion and the signal-to-noise ratio of the spectrum. The underestimate of the continuum level is naturally smaller for narrower lines (lower  $\sigma$ ), because the lines are detected and eliminated from the continuum estimation for lower values of  $W_0$ .

To summarize, the three tests of our continuum fitting methods presented in this Appendix demonstrate that the spline fitting method suffers from several systematic errors. The first test shows that a small negative absorption, of equivalent width  $\sim -0.3 \text{ km s}^{-1}$ , is induced where there is none. The second test indicates that the equivalent widths of strong, detected systems is overestimated by 10 – 20%. Finally, the third test shows that for weak systems, the continuum is systematically underestimated, thereby strongly reducing the contribution of these systems to the measured equivalent width. However, the

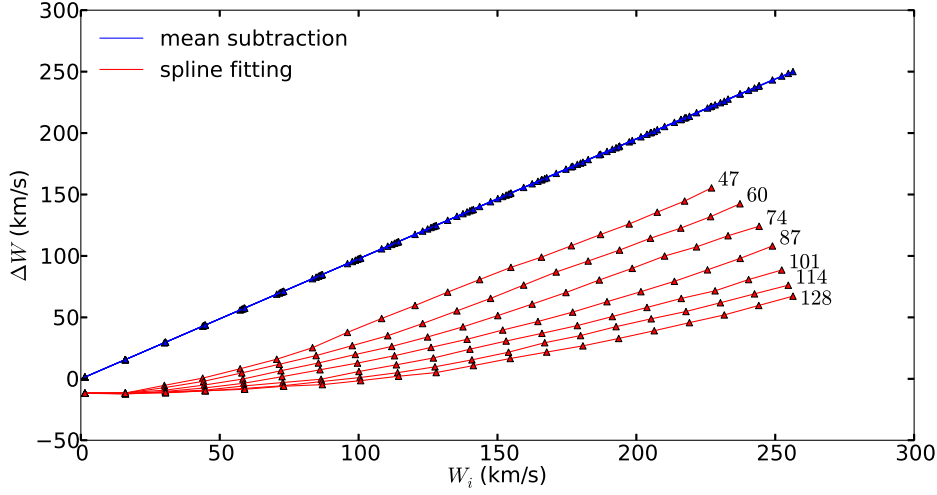


FIGURE 14. Change in the measured equivalent width,  $\Delta W$ , caused by the insertion of an absorbing system with equivalent width  $W_i$ , for the mean subtraction method (blue lines) and the spline fitting method (red lines). Results are shown as a function of the velocity dispersion  $\sigma$ , with values indicated to the right of the lines in km/s. The blue lines all nearly coincide at  $\Delta W = W_i$ . Points show the values of  $W_i$  for which  $\Delta W$  has been computed; the sudden changes in the red lines indicate discontinuities in the spline fitting method as the inserted line becomes detected or covers different pixels, which causes a change in the continuum estimate.

mean subtraction method successfully passes all these tests and should therefore provide a reliable estimate of the stacked equivalent width as a function of impact parameter.